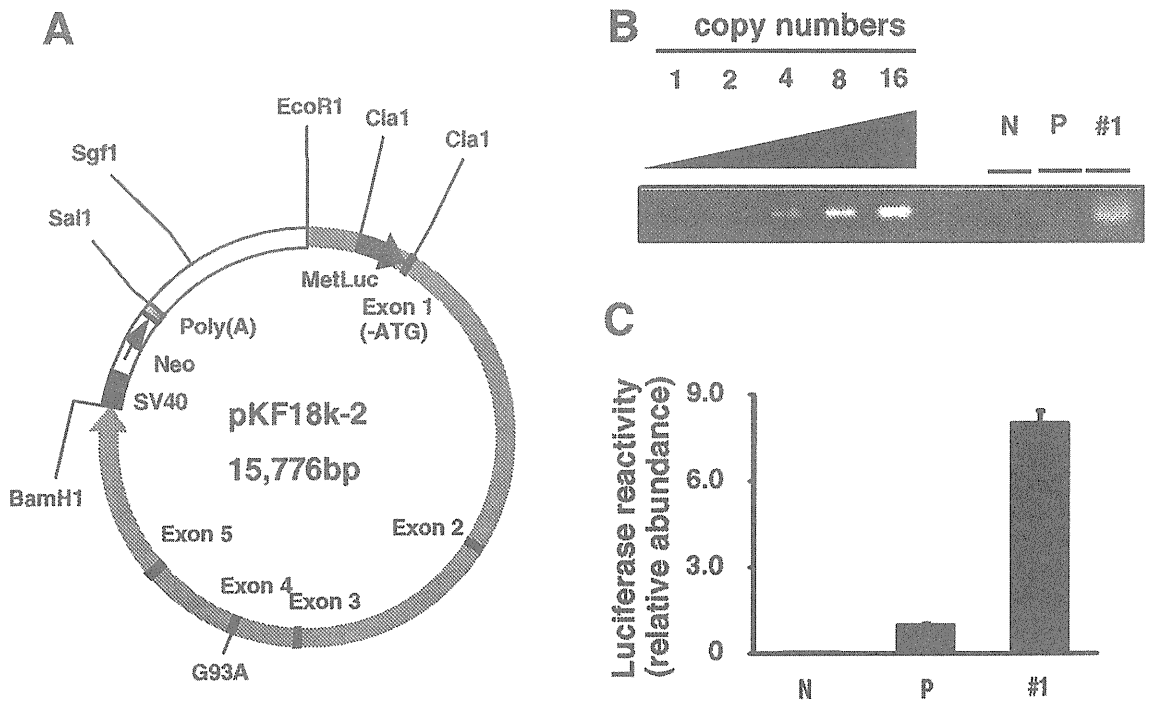

FIG. 1. The stable gPr^{SOD1}-Luc cell line used for the high-throughput screening (HTS) assay of compounds that downregulate SOD1 transcription. **(A)** Diagram of the superoxide dismutase gene (SOD1) promoter-luciferase reporter plasmid, which encodes a secreted luciferase incorporated into the human SOD1 gene, including the 5′- and 3′-untranslated region and introns. **(B)** Southern blotting analysis of the gPr^{SOD1}-Luc cell line. Clone 1 was the stable clone used in HTS assays. N, negative control, nontransfected H4 cells; P, positive control, H4 cells transiently transfected with the same cassette as clone 1. Copy number indicates the number of the transgene loaded. **(C)** Results of the luciferase reporter assay. Clone 1 has a relatively high number of copies of the transgene and, therefore, high luciferase activity. Values are mean ± SEM.

transgenic mice. The cassette was identical to that carried by $SOD1^{G93A}$ transgenic mice (gPr^{SOD1}-Luc), to reflect physiological activity of the SOD1 promoter (**Fig. 1A**). A total of 1.2 Kb of human SOD1 (hSOD1) 5′-fragment, with 5′-EcoR1 and 3′-Afe1-BamH1 sites, was amplified using PfuUltra 2 Fusion HS DNA Polymerase (Stratagene, Cedar Creek, TX). The following PCR primers were used to amplify the region: forward primer, 5′-AAAGAATTCTGCCAACCAAATAAG-3′; reverse primer, 5′-TTTGGATCCAGCGCTGAAGCCGGAAAGCGGAG-3′. The fragment was cloned into pKF18k-2 plasmid (Takara, Otsu, Japan). To add the Cla1 site and delete the start codon of SOD1 exon 1, the cassette was amplified by PfuUltra 2 Fusion HS DNA Polymerase using the following PCR primers: forward primer, 5′-GTTATCGATGCGACGAAGGCCGTGT-3′; reverse primer, 5′-TCGCTAGGCCACGCCGAGG-3′. The fragment was cut with EcoR1 and Afe1 and cloned into pKF18k-2-$hSOD1^{G93A}$. The SV40-Neo-Poly(A) was incorporated downstream from the SOD1 gene, between the BamH1 and Sal1 sites. Finally, secreted luciferase gene (MetLuc) from the marine copepod, *Metridia longa* (Clontech, Mountain View, CA), with ATG was added at the Cla1 site.

Human astrocytoma-derived H4 cells,[11] which are frequently used for research on neurodegenerative diseases,[12] were used for transfection to mimic the transcription of SOD1 in astrocytes. The cell lines were cultured at 37 °C in Dulbecco's modified Eagle's medium (DMEM; Sigma, St. Louis, MO), containing 10% (v/v) fetal bovine serum (FBS), 50 U mL^{-1} penicillin, 50 μg mL^{-1} streptomycin, and 200 μg mL^{-1} G418 (Nacalai, Kyoto, Japan). The cells were stably transfected with the SOD1 genomic construct cut by Sgf1, using FuGENE 6 Transfection Reagent (Roche, Basel, Switzerland). Clonal cell lines were selected based on high levels of secreted luciferase genes, and reactivity was confirmed by Southern blotting and luciferase reporter assay (**Fig. 1B,C**). For the Southern blotting, 15 μg DNA, cut at EcoR1 and BamH1, was loaded, and the probe was made from the following primers: forward primer, 5′-ATCTGGGAGACCATGGAAGT-3′; reverse primer, 5′-TTCTTTGAAGCCGCTGATCTC-3′.

The compound library

High-throughput screening (HTS) assays using the gPr^{SOD1}-luciferase cell line were performed to screen a library of 9600

compounds provided by the Institute for Chemical Research, Kyoto University. The library was delivered in 96-well racks, with each compound dissolved in DMSO at 5 mM. The extreme right and left wells contained DMSO without any compound, leaving the corresponding well on assay plates available for controls. All compounds were stored at −20 °C.

HTS assay

Luciferase expression by the gPr^{SOD1}-luciferase cells after exposure to various small compounds was assayed in white, flat-bottomed, 96-well plates (Costar, Bethesda, MD). The cells were precultured overnight at 3.0×10^4 cells $well^{-1}$ and 37 °C. The compound to be tested was preplated, diluted with culture medium to 50 μM, and used to replace 80 μL of 100 μL per well of cell culture to give a final concentration of 40 μM. The cells were then cultured for another 16 h at 37 °C.

SOD1 gene expression by cells exposed to each compound was determined by measuring activity of luciferase proteins secreted by the cells. The cell culture in each well was transferred to the corresponding well on a 96-well assay plate, using a Multifunction Tabletop Dispenser EDR-384S2 (Biotec, Tokyo, Japan). Ready-To-Glow Secreted Luciferase Reporter System (Clontech) was added, and luciferase activity was measured as emission at 450 nm, using a 1420 VICTOR 3 Multilabel Plate Reader with optional dispenser (PerkinElmer Life and Analytical Sciences, Waltham, MA). The ratios of the vehicle-treated samples were used to correct for spontaneous decay of the signal.

Assay performance was determined by calculating the Z factor (Z'), using the following equation:

$$Z' = 1 - \frac{3 \times (\sigma_{C+} + \sigma_{C-})}{(\mu_{C-} - \mu_{C+})},$$

where μ_{C+} and σ_{C+} are the mean and standard deviation (SD), respectively, of the positive control; μ_{C-} and σ_{C-} are the mean and SD of the negative control. The positive control assays treated cells with 10 μg mL^{-1} mitomycin-C (Wako, Osaka, Japan).[13] The negative control assays treated cells with vehicle (DMSO). The Z' value indicates the quality of an assay by describing the magnitude of the signal window ($\mu_C - \mu_{C+}$) and the precision of the assay ($\sigma_{C+} + \sigma_{C-}$). A compound was selected as a hit when it decreased luciferase activity less than mean minus 3 SD of negative controls. In each run, four or five library plates were applied to the screening assay with an individual control plate for calculating Z' value as well as an average and SD of luciferase activity for negative control. Hits were not selected from runs with a Z' value less than zero. The effect of hit compounds on the SOD1 expression was confirmed when it also decreased luciferase activity less than mean minus 3 SD of negative controls in duplicate by another assay.

Dose response and cytotoxicity

Dose–response analysis was carried out using the gPr^{SOD1}-luciferase cell line to confirm that the hit compounds reduced SOD1 expression in a dose-dependent manner. As in the primary assays, the cells were precultured overnight, and then the media were exchanged to give a 0- to 80-μM range of compound concentrations. The cells were incubated for another 16 h, and luciferase activity was measured. Only compounds that resulted in greater than −3 SD inhibition of SOD1 expression at 40 μM were included in further analyses because the concentration was also adapted for HTS assay selection.

Toxicity assays identified compounds that produced a nonspecific decrease in luciferase activity due to cellular toxicity. Toxicity analysis was performed on untransfected H4 cells, using the tetrazolium salt, WST-1 (Roche). In this assay, cleavage of WST-1 to formazan by mitochondrial dehydrogenases causes a color change from red to yellow. As in the primary assays, untransfected H4 cells were precultured overnight in a 96-well plate, and then the media were exchanged to give a 0- to 40-μM range of compound concentrations. The cells were incubated for 16 h, then WST-1 was added at 10 μL $well^{-1}$, and the cells were incubated for 1 h at 37 °C. Absorbance at 450 nm was compared to that of cells that were not treated with the compound. Compounds were considered to have significant cellular toxicity if cells treated with 40 μM showed greater than a −2 SD decrease in fluorescence compared to untreated cells.

Secondary assay

Enzyme-linked immunosorbent assays (ELISAs) and Western blots were used to determine whether effects observed in the reporter cell line could be reproduced at the level of endogenous SOD1 protein. As in the primary assays, untransfected H4 cells were precultured overnight, and the media were exchanged with hit compounds to give final concentrations of 0 to 40 μM. The cells were cultured for 48 h, and then each well was washed once with 200 μL of phosphate-buffered saline (PBS) and lysed with 100 μL of 1% Triton-X containing protease inhibitors (Roche).

ELISAs were performed to quantify differences in SOD1 protein levels, and EC_{50} values were calculated using a two-antibody sandwich ELISA for human SOD1. Polystyrene, enzyme-linked, immunosorbent, 96-well assay plates (Greiner Bio-one, Frickenhausen, Germany) were coated with 0.02 μg 0.1 mL^{-1} $well^{-1}$ of rabbit anti-SOD1 antibody (1:5000; cat. #SOD100; Stressgen, Ann Arbor, MI) in 50 mM sodium carbonate buffer at pH 9.4. The plates were incubated overnight at 4 °C. The wells were washed with PBS and blocked for 2 h with 3% bovine serum albumin (BSA) in wash buffer (PBS containing 0.05% Tween-20). The blocking solution was discarded; 50 μL of cell lysate diluted 1:100 in 3% BSA in wash buffer was added

to each well, along with recombinant SOD1 protein[14] (standard curve); and the plates were incubated overnight at 4 °C. The wells were washed with PBS, 100 µL of mouse anti-SOD1 antibody (1:1000; cat. #S2147; Sigma) was added, and the plates were incubated for 1 h at room temperature (RT). The wells were washed with PBS, and the bound mouse antibody was detected with 100 µL per well of horseradish peroxidase (HRP)–conjugated goat anti-mouse IgG antibody (1:5000; cat. #NA9310V; GE Healthcare, Buckinghamshire, UK). The plate was incubated for 1 h at RT and then reacted for 30 min with OptEIA TMB Substrate Reagent Set (BD Biosciences, San Jose, CA). The reaction was stopped by adding 100 µL of 1 M sodium phosphate. The rate of change in absorbance at 450 nm was measured with a ThermoFischer Scientific Multiskan JX (Thermo Electron Corporation, Waltham, MA). The concentration of SOD1 in the cell lysates was derived from a standard curve with a linear concentration range of 1.0 to 125 ng mL^{-1}.

The cell lysates were subjected to sodium dodecyl sulfate polyacrylamide gel electrophoresis (SDS-PAGE) and transferred to polyvinylidene difluoride membranes. Membranes were blocked in 3% BSA in TBS, probed with anti-SOD1 antibody (1:1000; Stressgen), and then reprobed with an anti-β-actin antibody (1:5000; cat. #A1978; Sigma) as an internal control.

Western blot analysis for phosphorylation of transcription factors

Untransfected H4 cells were precultured overnight on 12-well plates at 5.0×10^4 cells. The hit compound was diluted with culture medium to 25 µM and 50 µM and used to replace 0.8 mL of 1 mL per well of cell culture to give a final concentration of 20 µM and 40 µM, respectively. The cells were then cultured for another 16 h, and then each well was washed once with 2 mL PBS and lysed with 100 µL of 1% Triton-X containing protease inhibitors (Roche) and phosphatase inhibitor cocktail (Nacalai Tesque, Kyoto, Japan). Western blotting was performed with antibody specific to Ser^{40}-phosphorylated Nrf2 (2500:1; #EP1809Y; Abcam, Cambridge, MA), Nrf2 (500:1; H-300; #sc13032; Santa Cruz Biotechnology, Santa Cruz, CA), Ser^{133}-phosphorylated cAMP response element binding protein (CREB; 500:1; #06-519; Millipore, Billerica, MA), CREB (1000:1; #9197; Cell Signaling, Salem, MA), and β-actin (1:5000; Sigma).

Synthesis of 052C9

6-Chloro-3-formylchromone (0.20 g, 0.96 mmol) and o-phenylene diamine (0.10 g, 0.96 mmol) were dissolved in acetic acid (5 mL). The reaction mixture was stirred at 60 °C for 16 h and then diluted with an aqueous solution of $NaHCO_3$ (20 mL). The resulting precipitate was filtered and washed with water. The residue was dissolved in trifluoroacetic acid (1 mL) and then concentrated in vacuum. To the residue was added EtOAc (3 mL), and the resulting suspension was filtered to give 052C9 (72 mg, 18%) as a trifluoroacetic acid salt.

Table 1. Z′ of All the Runs

Run No.	*Z′*
1	0.69
2	0.39
3	0.35
4	0.55
5	0.60
6	0.38
7	0.42
8	0.38
9	0.37
10	−0.04
11	0.47
12	0.46
13	0.51
14	0.38
15	0.32
16	0.40
17	0.75
18	0.52
19	0.33
20	0.12
21	0.55

Table 2. Hit Compounds Identified Using the High-Throughput Screening Assay

	No. (%)
Screened compounds	9600
Total hits	325 (3.39)
Duplicate	141 (1.47)
Dose dependency	120 (1.25)
Toxic hits	5
Analysis continuing	115 (1.20)

Hits with dose dependency were defined as compounds that reduced luciferase activity in a dose-dependent manner, with a significant effect at least at 40 µM. Toxic hit compounds also decreased reporter activity in the WST-1 assay.

RESULTS

HTS assays using the gPr^{SOD1}-Luc cell line

As evidenced by the reduction in luciferase activity (**Fig. 1B,C**), the stable gPr^{SOD1}-Luc cell line expresses secreted luciferase under the control of a genomic SOD1 promoter and, therefore, is useful for identifying compounds that decrease SOD1 expression transcriptionally. The HTS assays using the gPr^{SOD1}-Luc cell line exhibited good reproducibility, with an average Z′ value of 0.39 (range, −0.23 to 0.75). Only two runs had Z′ values below zero (**Table 1**). We did not select hit compounds from these two runs. The effect of each compound was represented as the degree of inhibition of luciferase activity compared to vehicle-treated cells (**see Supplemental Figure 1**).

Using the HTS assay, duplicate assay, and dose-dependent testing, we identified 120 hit compounds that significantly inhibited SOD1 transcription (**Table 2**). We excluded the compounds with

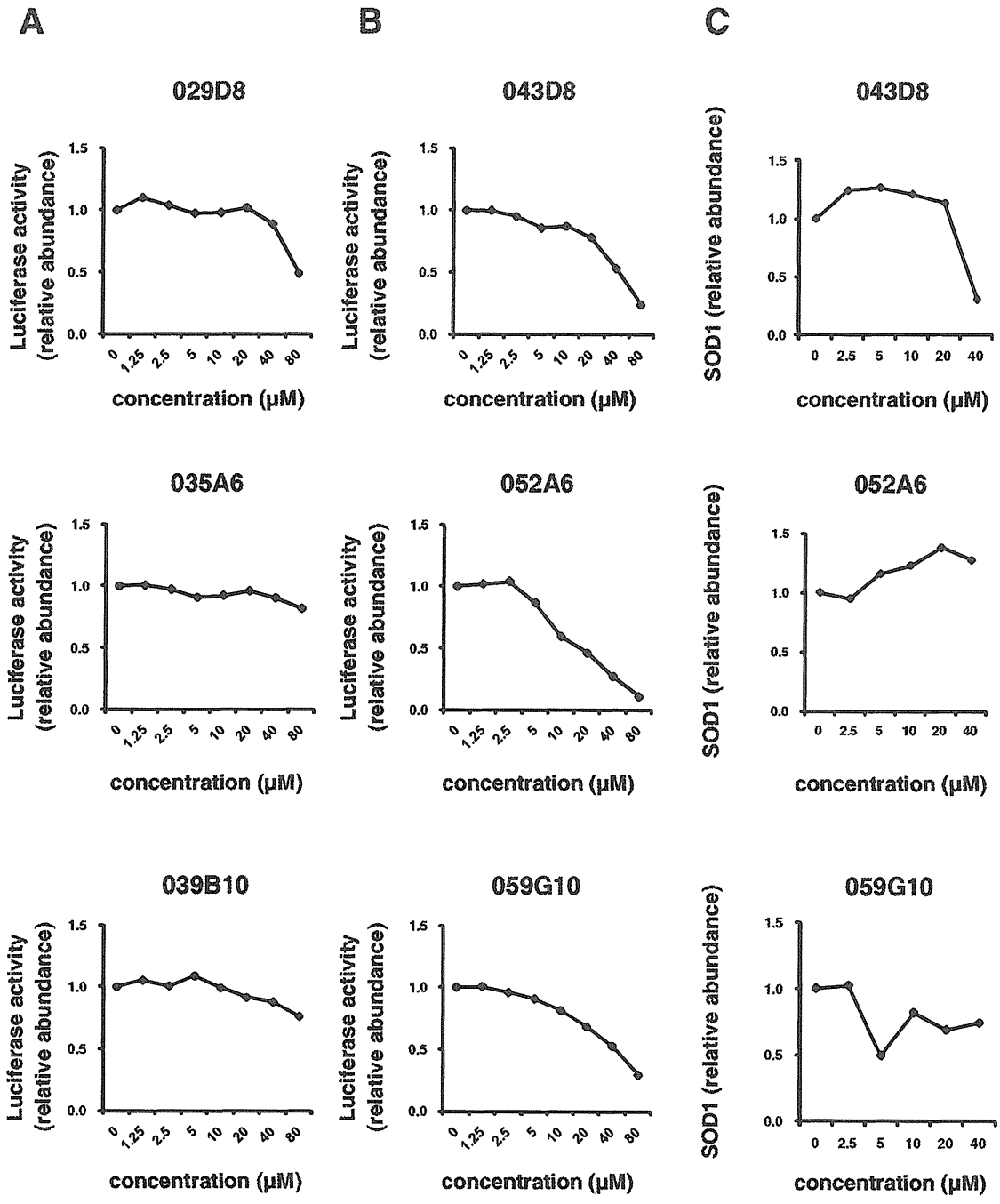

FIG. 2. (A) Representatives of dose-dependent effects of the excluded compounds on luciferase activity in gPr^{SOD1}-Luc cells. (B) Representatives of dose-dependent effects of compounds excluded by enzyme-linked immunosorbent assay (ELISA) on luciferase activity in gPr^{SOD1}-Luc cells. (C) Representatives of ELISA results of compounds excluded by ELISA on SOD1 abundance in H4 cells. Each point is the mean of duplicate measurements.

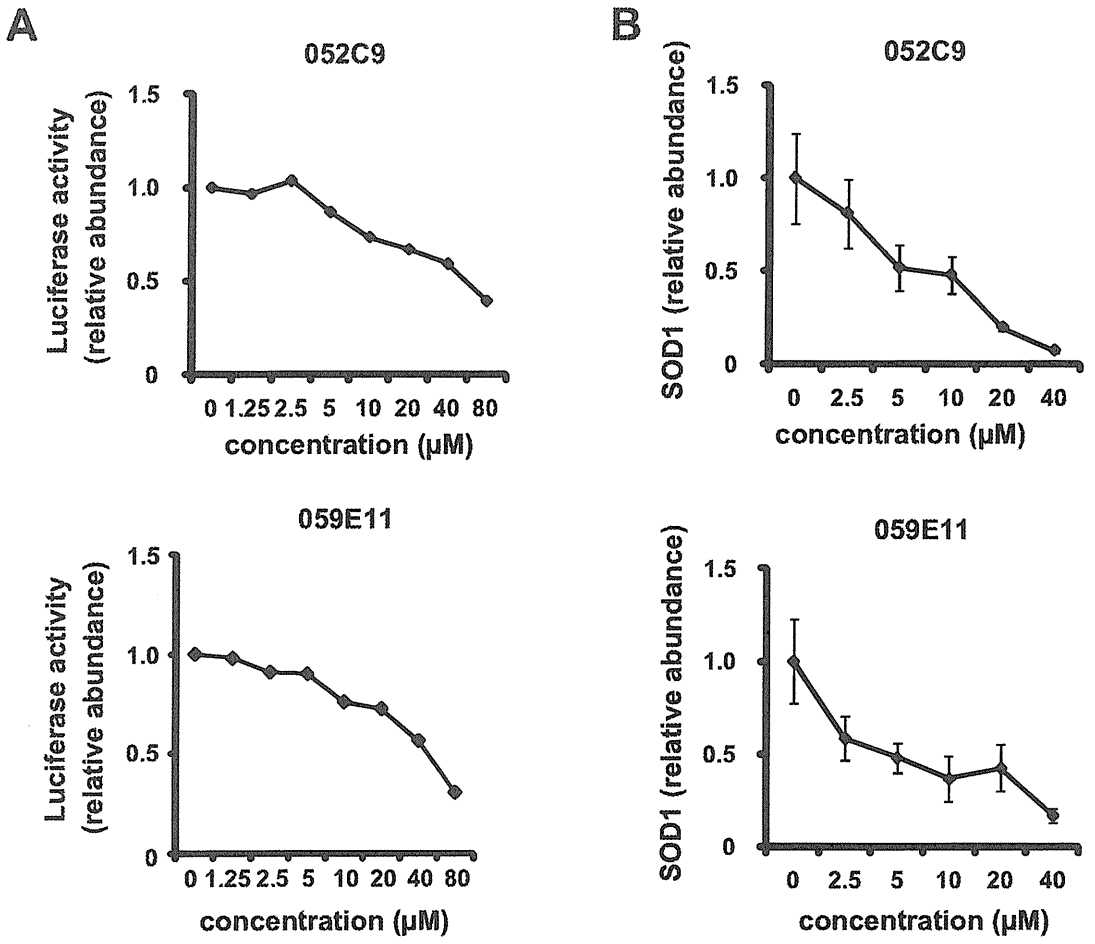

C

Hit Compounds through SOD1-ELISA

Compound	EC_{50}(μM)	TC_{50}(μM)
052C9	7.3	>40
059E11	19.6	>40

FIG. 3. (A) Dose-dependent effects of the hit compounds on luciferase activity in gPr^{SOD1}-Luc cells. Each point is the mean of duplicate measurements. (B) Enzyme-linked immunosorbent assay (ELISA) results showing effects of different concentrations of the two hit compounds on SOD1 expression. Values are means ± SEM (n = 5). (C) Hit compounds identified through SOD1-ELISA. EC_{50} = 50% effective concentration. TC_{50} = 50% toxic concentration.

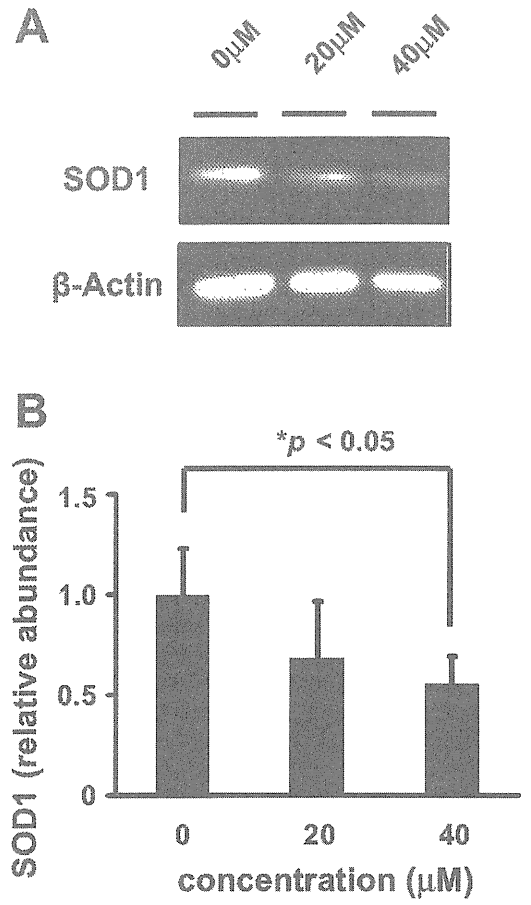

FIG. 4. (A) Representative Western blot showing the effect of different concentrations of the selected hit compound, 052C9, on expression of SOD1 and β-actin in H4 cells. (B) Band density of SOD1 relative to β-actin. Values are means ± SEM (n = 5). Difference between relative abundance at 0 and 40 μM was significant at $p < 0.05$ (one-way analysis of variance followed by the Bonferroni post hoc test).

poor dose-dependent responses (**Fig. 2A**). WST-1 assays indicated that five of these hit compounds had nonspecific cell toxicity (data not shown). ELISA results showed that 2 of the remaining 115 compounds reduced the level of endogenous SOD1 protein in a dose-dependent manner. We did not employ the compounds with no significant decline of SOD1 protein by ELISA (**Fig. 2B,C**). One of the compounds, 052C9, was selected for Western blot analysis, based on its downregulation of SOD1 expression, determined by the reporter assay (**Fig. 3A**) and by ELISA (**Fig. 3B**) with the lower 50% effective concentration (EC_{50}) compared to the other compound (**Fig. 3C**). The selected compound significantly decreased the level of endogenous SOD1 protein in H4 cells, with no reduction in expression of β-actin (**Fig. 4**). The structure of this hit compound (**Fig. 5**) was confirmed by resynthesis and spectroscopic characterization: The molecule is composed of a benzoimidazole ring and a chroman unit and is not analogous to any of the drugs used in ALS treatment trials to date. Two major transcription factors have been reported to activate the expression of SOD1: NF-E2 (Nrf2) and CREB. We examined the effects of 052C9 on the phosphorylation status of these two transcription factors by Western blot analysis. The results showed that 052C9 blocked the phosphorylation of NF-E2 (Nrf2) with no reduction of total Nrf2 protein level, whereas 052C9 had no detectable effects on the phosphorylation status of CREB (**Fig. 6**).

DISCUSSION

In a recent article, Broom et al.[15] developed HTS assays to identify compounds that downregulate SOD1 expression. On the basis of this previous study, we executed the present study targeting the transcription of SOD1 with a different compound library and a modified reporter construct of SOD1 promoter. The HTS system using astrocytoma-derived H4 cells successfully identified a number of hit compounds that decrease the expression of SOD1 protein. The HTS assays exhibited good reproducibility, with an average Z′ value of 0.39 (range, −0.23 to 0.75). This variability might be due to the manual preplating of the cells for screening or the instability of the secreted luciferase. Although the assay results had a high coefficient of variation, this could be attributed to the relatively high abundance of hit compounds (3.39%; **Table 2**). Because this hit percentage may partially reflect Gaussian statistics, we confirmed the significant efficacy of the hit compounds on SOD1 expression through another duplicate assay and dose-dependent analysis. This process would allow us to rule out the effect of Gaussian statistics on the hit selection. Although most of the hit compounds failed to decrease endogenous SOD1 protein level by ELISA in a dose-dependent manner, we suppose that this may be due to direct inhibition of luciferase reaction or to the difference between temporal patterns of the transcription and translation of SOD1. At least one of the hit compounds, 052C9, significantly downregulated SOD1 protein levels in a dose-dependent manner. It is unlikely that the effect reflects nonspecific cellular toxicity because the WST-1 assay showed no significant effects at the concentrations at which the compound exerted the downregulation of SOD1. It is also unlikely that the hit compound represses transcription generally, as there was no corresponding reduction in expression of β-actin.

The mode of action of 052C9 remains unclear at the moment. Nevertheless, our analysis suggests that 052C9 directly or indirectly blocks the phosphorylation of Nrf2. Transcription factor Nrf2 binds to the antioxidant response element (ARE) in the promoter region of detoxifying genes.[16] Phosphorylation of Nrf2 promotes its translocation into the nucleus where it activates the transcription of antioxidant genes.[17] Because the SOD1 gene also

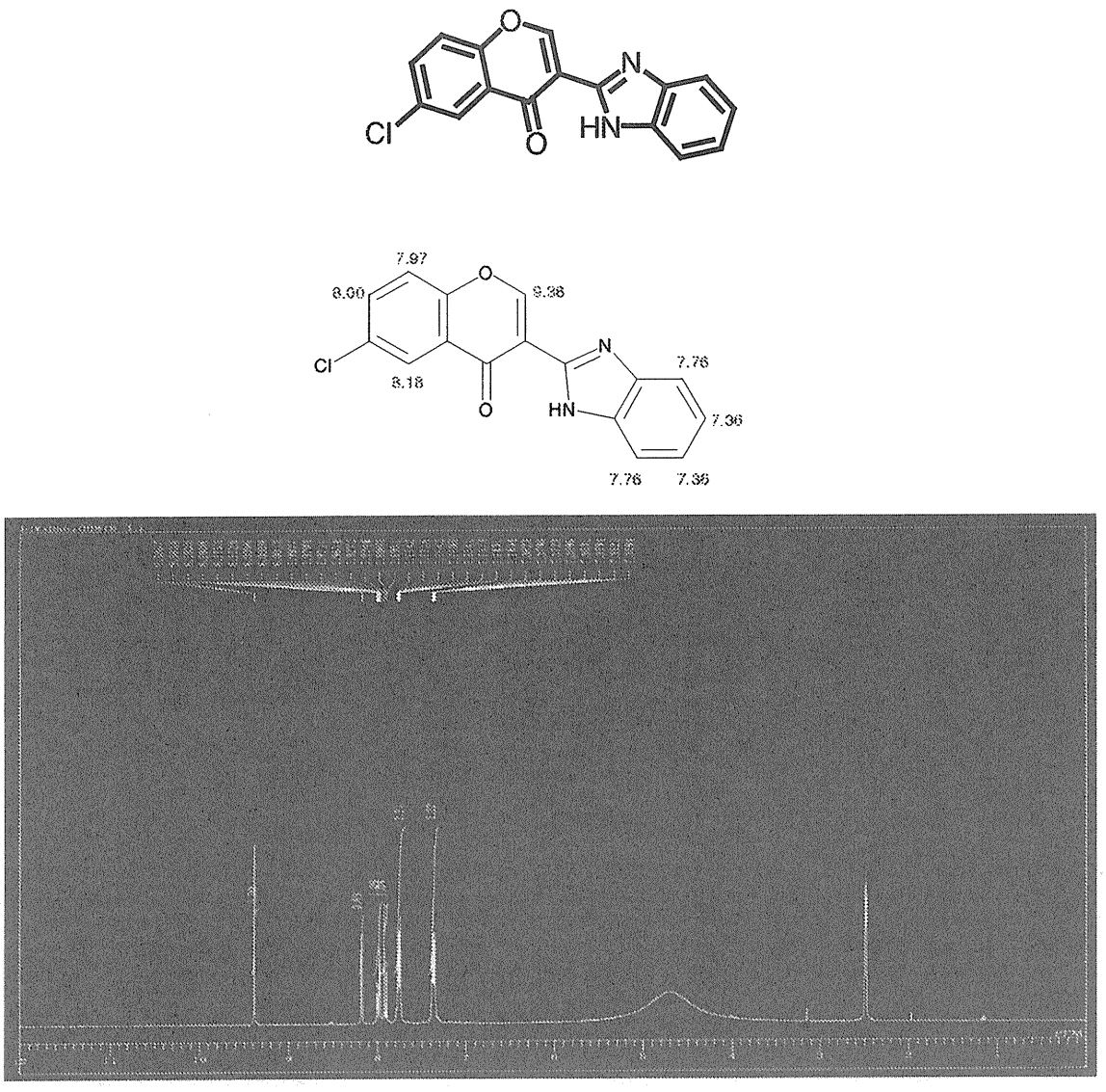

FIG. 5. The chemical structure of the selected hit compound.
^{1}H NMR (DMSO-d_6, 300 MHz) delta-$_H$ 9.38 (d, J = 1.1 Hz, 1H), 8.18 (d, J = 2.7 Hz, 1H), 7.99 (dd, J = 9.1, 2.7 Hz, 1H), 7.91 (dd, J = 9.1, 1.1 Hz, 1H), 7.76 (dd, J = 6.0, 3.0 Hz, 2H), 7.36 (dd, J = 6.0, 3.0 Hz, 2H)
^{13}C NMR (DMSO-d_6, 75 MHz) delta-$_C$ 172.9 (s), 160.0 (d), 154.1 (s), 143.5 (s), 135.2 (s), 134.4 (s × 2), 131.3 (s), 124.4 (d), 124.3 (d × 2), 124.3 (d), 121.4 (d), 114.8 (d), 111.7 (s) MS (ESI) mass calcd for $C_{16}H_9ClN_2O_2$ + H requires m/z 297 Found m/z 297

contains ARE,[18] the hit compound, 052C9, may downregulate the transcription of SOD1 by inhibiting phosphorylation of Ser^{40} of Nrf2. 052C9 had no detectable effects on the Ser^{133} phosphorylation of CREB in the present study. Because protein kinase C (PKC) phosphorylates both of the two transcription factors,[17,19] it is likely that 052C9 inhibits the activity of an unidentified Nrf2-selective kinase or its activation. 052C9 or its analogs may serve as a powerful tool for exploring the molecular mechanism of SOD1 expression.

The hit compounds identified in the present study cause a partial reduction in SOD1 expression. Although the effects on ALS-model mice have not yet been examined, partial downregulation

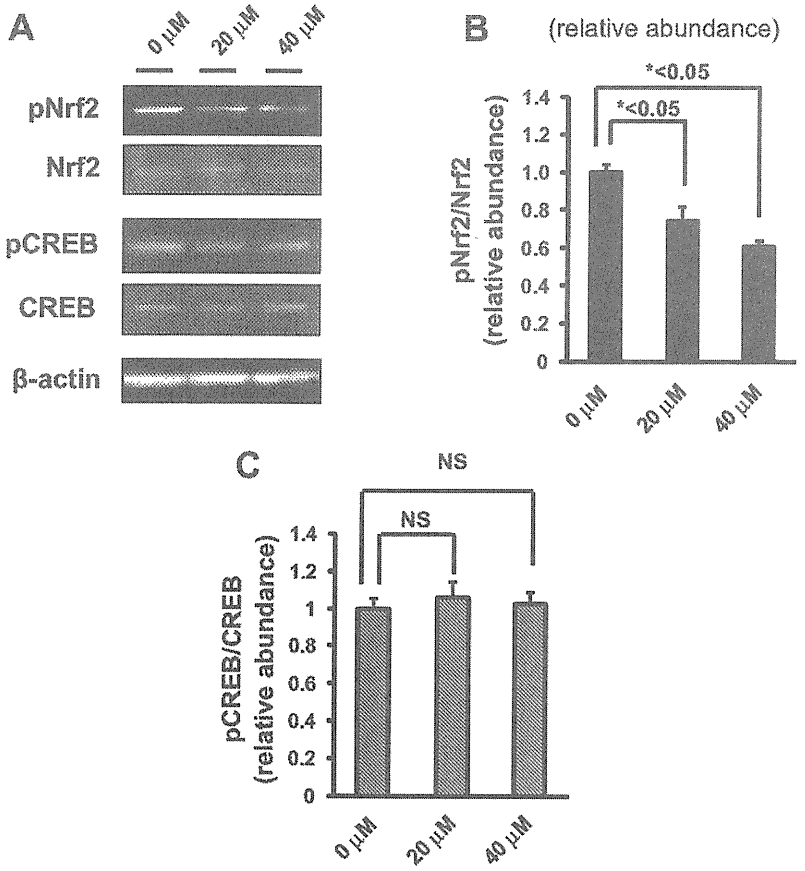

FIG. 6. (A) Representative Western blot showing the effect of different concentrations of the selected hit compound, 052C9, on phosphorylation of Nrf2 and cAMP response element binding protein (CREB) in H4 cells. (B) Band density of pNrf2 relative to Nrf2. Values are means ± SEM ($n = 7$). Differences between relative abundance both at 0 and 20 μM and at 0 and 40 μM were significant at $p < 0.05$ (one-way analysis of variance [ANOVA] followed by the Bonferroni post hoc test). (C) Band density of pCREB relative to CREB. Values are means ± SEM ($n = 7$). Differences between relative abundance both at 0–20 μM and at 0–40 μM were not significant (one-way ANOVA followed by the Bonferroni post hoc test).

of SOD1 expression may be desirable. SOD1-knockout mice do not develop the motor neuron disease phenotype[3] but do show modest vulnerability to axotomy[3] and pathological degeneration of neuromuscular junctions and axons.[20]

Decreasing wild-type SOD1 by a small molecule may prove to alleviate the disease phenotype in ALS-model mice and even in sporadic ALS patients. A previous study showed that wild-type (WT) SOD1 transgenic mice have pathological changes similar to those in mutant SOD1 mice and that WT SOD1 aggravates the ALS phenotype in double-transgenic mice with both WT-SOD1 and mutant SOD1.[21] Moreover, the mutation in the SOD1 promoter reduces SOD1 gene expression and may correlate with a delay in the onset of sporadic ALS.[22] Indeed, Zhong et al.[23] reported that administration of activated protein C (APC) to mutant SOD1 mice, which decreases the expression of SOD1 protein *in vivo*, ameliorates the ALS phenotype. Based on these findings, the toxicity of mutant SOD1 may not be explained by a gain of toxic function but by an increased toxicity of wild-type SOD1. Direct reduction of the transcription of pathogenic SOD1 protein may provide a new therapeutic strategy for SOD1-mediated ALS, and similar strategies may be used to treat other neurodegenerative diseases mediated by aberrant proteins.

ACKNOWLEDGMENTS

This work was supported by research grants from the Ministry of Health and Labour (R.T., H.I.), the New Energy and Industrial Technology Development Organization (NEDO)

(N.N.), JSPS (21591079) (H.I.), and JST (M.U.). We thank Ryoichi Nakano for providing the pHGSOD-Svneo plasmid and Kazumi Murai for editing the manuscript.

REFERENCES

1. Rosen, D. R.; Siddique, T.; Patterson, D.; Figlewicz, D. A.; Sapp, P.; Hentati, A.; Donaldson, D.; Goto, J.; O'Regan, J. P.; Deng, H.-X.; et al. Mutations in Cu/Zn Superoxide Dismutase Gene Are Associated with Familial Amyotrophic Lateral Sclerosis. *Nature* **1993**, *362*, 59–62.
2. Gurney, M. E.; Pu, H.; Chiu, A. Y.; Dal Canto, M. C.; Polchow, C. Y.; Alexander, D. D.; Caliendo, J.; Hentati, A.; Kwon, Y. W.; Deng, H. X.; et al. Motor Neuron Degeneration in Mice That Express a Human Cu/Zn Superoxide Dismutase Mutation. *Science* **1994**, *264*, 1772–1775.
3. Reaume, A. G.; Elliott, J. L.; Hoffman, E. K.; Kowall, N. W.; Ferrante, R. J.; Siwek, D. F.; Wilcox, H. M.; Flood, D. G.; Beal, M. F.; Brown, R. H., Jr.; et al. Motor Neurons in Cu/Zn Superoxide Dismutase-Deficient Mice Develop Normally but Exhibit Enhanced Cell Death after Axonal Injury. *Nat. Genet.* **1996**, *13*, 43–47.
4. Nagai, M.; Aoki, M.; Miyoshi, I.; Kato, M.; Pasineli, P.; Kasai, N.; Brown, R. H., Jr.; Itoyama, Y. Rats Expressing Human Cytosolic Copper-Zinc Superoxide Dismutase Transgenes with Amyotrophic Lateral Sclerosis: Associated Mutations Develop Motor Neuron Disease. *J. Neurosci.* **2001**, *21*, 9246–9254.
5. Yamanaka, K.; Chun, S. J.; Boillee, S.; Fujimoto-Tonou, N.; Yamashita, H.; Gutmann, D. H.; Takahashi, R.; Misawa, H.; Cleveland, D. W. Astrocytes as Determinants of Disease Progression in Inherited Amyotrophic Lateral Sclerosis. *Nat. Neurosci.* **2008**, *11*, 251–253.
6. Boillee, S.; Yamanaka, K.; Lobsiger, C. S.; Copeland, N. G.; Jenkins, N. A.; Kassiotis, G.; Kollias, G.; Cleveland, D. W. Onset and Progression in Inherited ALS Determined by Motor Neurons and Microglia. *Science* **2006**, *312*, 1389–1392.
7. Saito, Y.; Yokota, T.; Mitani, T.; Ito, K.; Anzai, M.; Miyagishi, M.; Taira, K.; Mizusawa, H. Transgenic Small Interfering RNA Halts Amyotrophic Lateral Sclerosis in a Mouse Model. *J. Biol. Chem.* **2005**, *280*, 42826–42830.
8. Smith, R. A.; Miller, T. M.; Yamanaka, K.; Monia, B. P.; Condon, T. P.; Hung, G.; Lobsinger, C. S.; Ward, C. M.; McAlonis-Downes, M.; Wei, H.; et al. Antisense Oligonucleotide Therapy for Neurodegenerative Disease. *J. Clin. Invest.* **2006**, *116*, 2290–2296.
9. Yamamoto, A.; Lucas, J. J.; Hen, R. Reversal of Neuropathology and Motor Dysfunction in a Conditional Model of Huntington's Disease. *Cell* **2000**, *101*, 57–66.
10. Santacruz, K.; Lewis, J.; Spires, T.; Paulson, J.; Kotilinek, L.; Ingelsson, M.; Guimaraes, A.; DeTure, M.; Ramsden, M.; McGowan, E.; et al. Tau Suppression in a Neurodegenerative Mouse Model Improves Memory Function. *Science* **2005**, *309*, 476–481.
11. Krex, D.; Mohr, B.; Hauses, M.; Ehninger, G.; Schackert, H. K.; Schackert, G. Identification of Uncommon Chromosomal Aberrations in the Neuroglioma Cell Line H4 by Spectral Karyotyping. *J. Neuro-oncol.* **2001**, *52*, 119–128.
12. Kukar, T. L.; Ladd, T. B.; Bann, M. A.; Fraering, P. C.; Narlawar, R.; Maharvi, G. M.; Healy, B.; Chapman, R.; Welzel, A. T.; Price, R. W.; et al. Substrate-Targeting γ-Secretase Modulators. *Nature* **2008**, *453*, 925–930.
13. Broom, W. J.; Ay, I.; Pasinelli, P.; Brown, R. H., Jr. Inhibition of SOD1 Expression by Mitomycin C is a Non-Specific Consequence of Cellular Toxicity. *Neurosci. Lett.* **2006**, *393*, 184–188.
14. Urushitani, M.; Kurisu, J.; Tateno, M.; Hatakeyama, S.; Nakayama, K.; Kato, S.; Takahashi, R. CHIP Promotes Proteasomal Degradation of Familial ALS-Linked Mutant SOD1 by Ubiquitinating Hsp/Hsc70. *J. Neurochem.* **2004**, *90*, 231–244.
15. Broom, W. J.; Auwarter, K. E.; Ni, J.; Russel, D. E.; Yeh, L.; Maxwell, M. M.; Glicksman, M.; Kazantsev, A. G.; Brown, R. H., Jr. Two Approaches to Drug Discovery in SOD1-Mediated ALS. *J. Biomol. Screen.* **2006**, *11*, 729–735.
16. Nguyen, T.; Nioi, P.; Pickett, C. B. The Nrf2-Antioxidant Response Element Signaling Pathway and Its Activation by Oxidative Stress. *J. Biol. Chem.* **2009**, *284*, 13291–13295.
17. Huang, H. C.; Nguyen, T.; Pickett, C. B. Phosphorylation of Nrf2 at Ser40 by Protein Kinase C Regulates Antioxidant Response Element-Mediated Transcription. *J. Biol. Chem.* **2002**, *277*, 42769–42774.
18. Park, E. Y.; Rho, H. M. The Transcriptional Activation of the Human Copper/Zinc Superoxide Dismutase Gene by 2,3,7,8-Tetrachlorodibenzo-p-Dioxin through Two Different Regulator Sites, the Antioxidant Responsive Element and Xenobiotic Responsive Element. *Mol. Cell. Biochem.* **2002**, *24*, 47–55.
19. Johannessen, M.; Moens, U. Multisite Phosphorylation of cAMP Response Element-Binding Protein (CREB) by a Diversity of Protein Kinases. *Front Biosci.* **2007**, *12*, 1814–1832.
20. Flood, D. G.; Reaume, A. G.; Gruner, J. A.; Hoffman, E. K.; Hirsch, J. D.; Lin, Y.; Dorfman, K. S.; Scott, R. W. Hindlimb Motor Neurons Require Cu/Zn Superoxide Dismutase for Maintenance of Neuromuscular Junctions. *Am. J. Pathol.* **1999**, *155*, 663–672.
21. Jaarsma, D.; Haasdijk, E. D.; Grashorn, J. A. C.; Hawkins, R.; Duijn, W.; Verspaget, H. W.; London, J.; Holstege, J. C. Human Cu/Zn Superoxide Dismutase (SOD1) Overexpression in Mice Causes Mitochondrial Vacuolization, Axonal Degeneration, and Premature Motoneuron Death and Accelerates Motoneuron Disease in Mice Expressing a Familial Amyotrophic Lateral Sclerosis Mutant SOD1. *Neurobiol Dis.* **2000**, *7*, 623–643.
22. Broom, W. J.; Greenway, M.; Sadri-Vakili, G.; Russ, C.; Auwarter, K. E.; Glajch, K. E.; Dupre, N.; Swingler, R. J.; Purcell, S.; Hayward, C.; et al. 50bp Deletion in the Promoter for Superoxide Dismutase 1 (SOD1) Reduces SOD1 Expression In Vitro and May Correlate with Increased Age of Onset of Sporadic Amyotrophic Lateral Sclerosis. *Amyotroph. Lateral Scler.* **2008**, *9*, 229–237.
23. Zhong, Z.; Ilieva, H.; Hallagan, L.; Bell, R.; Singh, I.; Paquette, N.; Thiyagarajan, M.; Deane, R.; Fernandez, J. A.; Lane, S.; et al. Activated Protein C Therapy Slows ALS-Like Disease in Mice by Transcriptionally Inhibiting SOD1 in Motor Neurons and Microglia Cells. *J. Clin. Invest.* **2009**, *119*, 3437–3449.

Address correspondence to:
Haruhisa Inoue, M.D., Ph.D.
Center for iPS Cell Research and Application (CiRA)
Kyoto University 53 Shogoin Kawahara-cho,
Sakyo-ku, Kyoto, 606-8507, Japan

E-mail: haruhisa@cira.kyoto-u.ac.jp

and

Ryosuke Takahashi, M.D., Ph.D.
Department of Neurology, Graduate School of Medicine, Kyoto University
Kyoto University 54 Shogoin Kawahara-cho,
Sakyo-ku, Kyoto, 606-8507, Japan

E-mail: ryosuket@kuhp.kyoto-u.ac.jp

THE JOURNAL OF BIOLOGICAL CHEMISTRY VOL. 286, NO. 10, pp. 7947–7957, March 11, 2011

The Endoplasmic Reticulum Stress Sensor, ATF6α, Protects against Neurotoxin-induced Dopaminergic Neuronal Death*[S]

Received for publication, June 22, 2010, and in revised form, October 17, 2010 Published, JBC Papers in Press, December 3, 2010, DOI 10.1074/jbc.M110.156430

Naohiro Egawa[‡§], Keisuke Yamamoto[¶‖], Haruhisa Inoue[**], Rie Hikawa[‡§], Katsunori Nishi[‡‡], Kazutoshi Mori[§¶], and Ryosuke Takahashi[‡§1]

From the [‡]Department of Neurology, Graduate School of Medicine, Kyoto University, Kyoto 606-8507, Japan, [§]Core Research for Evolutional Science and Technology (CREST), Japan Science and Technology Corporation, Japan, the [¶]Department of Biophysics, Graduate School of Science, Kyoto University, Kyoto 606-8502, Japan, the [‖]Institute of Genome Research, Tokushima University, Tokushima 770-8503, Japan, the [**]Center for iPS Cell Research and Application (CiRA), Kyoto University, Kyoto 606-8507, Japan, and the [‡‡]Tokyo Metropolitan Institute for Neuroscience, Tokyo 183-8526, Japan

Oxidative stress and endoplasmic reticulum (ER) stress are thought to contribute to the pathogenesis of various neurodegenerative diseases including Parkinson disease (PD), however, the relationship between these stresses remains unclear. ATF6α is an ER-membrane-bound transcription factor that is activated by protein misfolding in the ER and functions as a critical regulator of ER quality control proteins in mammalian cells. The goal of this study was to explore the cause-effect relationship between oxidative stress and ER stress in the pathogenesis of neurotoxin-induced model of PD. 1-Methyl-4-phenyl-1,2,3,6-tetrahydropyridine (MPTP), a dopaminergic neurotoxin known to produce oxidative stress, activated ATF6α and increased ER chaperones and ER-associated degradation (ERAD) component in dopaminergic neurons. Importantly, MPTP induced formation of ubiquitin- immunopositive inclusions and loss of dopaminergic neurons more prominently in mice deficient in ATF6α than in wild-type mice. Cultured cell experiments revealed that 1-methyl-4-phenylpyridinium (MPP^+)-induced oxidative stress not only promoted phosphorylation of p38 mitogen-activated protein kinase (p38MAPK) but also enhanced interaction between phosphorylated p38MAPK and ATF6α, leading to increment in transcriptional activator activity of ATF6α. Thus, our results revealed a link between oxidative stress and ER stress by showing the importance of ATF6α in the protection of the dopaminergic neurons from MPTP that occurs through oxidative stress-induced activation of ATF6α and p38MAPK-mediated enhancement of ATF6α transcriptional activity.

Parkinson disease (PD)[2] is characterized pathologically by progressive and selective loss of dopaminergic neurons in the substantia nigra pars compacta (SNc). Recent studies have suggested some pathogenetic mechanisms of PD, including mitochondrial dysfunction (1), oxidative stress induced by dopamine metabolites, and endoplasmic reticulum (ER) stress induced by the accumulation of unfolded proteins (2–4). Dopaminergic neuron loss is often accompanied by formation of intraneuronal inclusion bodies termed Lewy bodies whose major constituent is α-synuclein (5), suggesting the pathogenetic role of unfolded protein accumulation and aggregation.

The unfolded protein response (UPR) is a homeostatic signaling pathway designed to cope with the accumulation of unfolded proteins in the ER lumen. In mammals, the UPR utilize three types of sensor proteins, PERK, IRE1α, and ATF6α, which detect protein-misfolding stress in the ER and initiate ER-to-nucleus signaling cascades to maintain the homeostasis of protein quality control system (6). ATF6 is a type 2 transmembrane protein; the C-terminal region is located in the ER, whereas the N-terminal region is located in the cytosolic side. ATF6 consists of two subtypes, ATF6α and ATF6β. ATF6α or ATF6β single knock-out mice normally develops but mice deficient in both subtypes of ATF6 genes showed embryonic lethal (7, 8). Upon ER stress the N-terminal fragment of ATF6α designated pATF6α(N) is cleaved from the parent protein designated pATF6α(P) and transported into the nucleus, where it binds to cis-acting ER stress response element (ERSE) and UPR element (UPRE), and up-regulates major ER chaperones and ER-associated degradation (ERAD) components (9–14).

1-Methyl-4-phenyl-1,2,3,6-tetrahydropyridine (MPTP) is converted into 1-methyl-4- phenylpyridinium (MPP^+) in astrocytes and taken up by dopaminergic neurons through the dopamine transporter (DAT). MPP^+ interferes with the mitochondrial complex-1, generates reactive oxygen species (ROS) and selectively damages dopaminergic neurons (15). Dopamine itself is also a highly-reactive molecule and naturally metabolized to produce ROS including hydrogen peroxide (H_2O_2) via the monoamine oxidase pathway (16). Dopamine-induced ROS promotes phosphorylation of p38 mitogen-activated protein kinase (p38MAPK) (17). MPTP activates p38MAPK pathway in the dopaminergic neuron (18). Other

* This study was supported in part by a grant-in-aid for scientific research on Priority Areas-Research on Pathomechanisms of Brain Disorders from the Ministry of Education, Culture, Sports, Science and Technology of Japan and a Grant-in-aid from the Ministry of Health, Labor, and Welfare of Japan.

[S] The on-line version of this article (available at http://www.jbc.org) contains supplemental Table S1 and Figs. S1–S3.

[1] To whom correspondence should be addressed: Dept. of Neurology, Kyoto University Graduate School of Medicine, 54 Shogoin-Kawahara-cho, Sakyo-ku, Kyoto 606-8507, Japan. Tel.: 81-75-751-3770; Fax: 81-75-761-9780; E-mail: ryosuket@kuhp.kyoto-u.ac.jp.

[2] The abbreviations used are: PD, Parkinson disease; ER, endoplasmic reticulum; MPTP, 1-methyl-4-phenyl-1,2,3,6-tetrahydropyridine; ERAD, ER-associated degradation; UPR, unfolded protein response; MPP^+, 1-methyl-4-phenylpyridinium.

oxidative neurotoxins such as rotenone and 6-hydroxydopamine (6-OHDA) also enhance the phosphorylation of p38MAPK (19, 20). Interestingly, it was previously reported that phosphorylated p38MAPK can regulate ATF6α function via phosphorylation (21), suggesting the possibility that oxidative stress and ER stress intersect at the level of p38MAPK and ATF6α.

Based on these data, the goal of the present study was to explore the cause-effect relationship between oxidative stress and ER stress in the pathogenesis of PD using ATF6α wild-type (WT) and knock-out (KO) mice treated with MPTP that causes oxidative stress and damages dopaminergic neurons.

EXPERIMENTAL PROCEDURES

Animal and MPTP Treatment—ATF6α knock-out (KO) mice were generated by gene targeting techniques as previously described (7). Groups of male ATF6α KO mice and wild-type (WT) littermate controls were injected intraperitoneal with 20 mg/kg of MPTP hydrochloride (Sigma-Aldrich) four times at 2 h intervals on the same day ($n = 10$ for each group). The mice were decapitated 5 days after injection for the subsequent analysis. All surgical procedures were performed according to the rules set forth by the Ethics Committee of Kyoto University.

Quantitative Real-time PCR—The mouse central nervous system (CNS) was dissected into the cerebral cortex, the brainstem, the hippocampus, the striatum, the midbrain, the cerebellum, the olfactory bulb, and the thalamus. Total RNA was isolated from the various parts of the CNS using the RNeasy Kit (Qiagen, Valencia CA) after homogenization (POLYTRON PT10–35). The first strand of cDNA was synthesized from 1 μg of total RNA using the PrimeScript RT Reagent Kit (Takara Bio, Shiga). Real-time PCR was performed using the LightCycler SYBR Green Master Kit and LightCycler 480 program (Roche) according to the manufacturer's protocol. The sequences of the primers used were listed in the supplemental Table S1. Values were normalized and expressed relative to GAPDH values.

Immunoblotting—Each part of the dissected CNS tissue was weighed and homogenized (POLYTRON PT10–35) in 1 ml/g of ice-cold buffer (50 mM Tris(pH7.5), 5 mM EDTA and 120 mM NaCl, 1% Triton X-100) containing protease inhibitor and phosphatase inhibitor mixture. Samples were centrifuged at 1,000 × *g* for 5 min, where the supernatant was collected for the additional centrifugation and the resulting pellet was dissolved in 2% SDS buffer for nuclear fraction. The supernatant was centrifuged at 165,000 × *g* for 60 min. The supernatant was prepared for cytosolic fraction, and the resulting pellet was dissolved in 2% SDS buffer as the ER and vesicle fraction. SH-SY5Y cells, HEK293T cells, ATF6α WT and ATF6α KO mouse embryonic fibroblasts (MEFs) were lysed in lysis buffer containing 1% Triton X-100 or 2% SDS buffer containing protease inhibitor and phosphatase inhibitor mixture. 20 or 30 μg of protein for each sample was separated by SDS-PAGE and electroblotted onto PDGF membrane (Immunopore). Immunoblotting analysis was carried out using an enhanced chemiluminescence Western blotting detection system kit (Amersham Biosciences). Rabbit anti-ATF6α polyclonal antibody was prepared as previously described (13). Mouse anti-BiP antibody was purchased from BD Biosciences (San Diego, CA). Rat anti-GRP94 antibody was purchased from Stressgen (Ann Arbor, MI). Rabbit anti-Derlin-3 antibody was purchased from Sigma-Aldrich. β-Actin antibody, anti-p38MAPK antibody, anti-phosho-p38MAPK (p-p38MAPK) antibody and anti-IRE1α antibody were obtained from Cell Signaling (Boston, MA). Rabbit anti-DAT antibody and mouse anti-tyrosine hydroxylase (TH) antibody were purchased from Millipore (Billerica, MA). Rabbit anti-ubiquitin antibody was purchased from DAKO (Glostrup, Denmark). Goat anti-PERK and rabbit anti-phospho-PERK antibody were obtained from Santa Cruz Biotechnology.

Immunohistochemistry—Mice were injected with pentobarbital and perfused transcardially with PBS, followed by 4% paraformaldehyde in PBS. Mice were decapitated, and their brains were removed and immersed in 4% paraformaldehyde in PBS for fixation. Serial coronal sections at 20-μm thickness were collected on slides. Deparaffinized sections were rinsed with PBS containing 0.1% Triton X-100 and then immersed in 0.3% H_2O_2 for 30 min. Sections were stained with primary antibodies against TH (mouse monoclonal; Millipore), BiP (IMGENEX, San Diego, CA) or ubiquitin (DAKO) or p-p38MAPK (Cell Signaling) in 10% normal serum overnight at 4 °C. After washing three times in PBST, the sections were stained with biotinylated secondary antibodies (Vector Laboratories, Burlingame, CA), using the standard avidin-biotin peroxidase method (Elite standard kit SK6100; Vector Laboratories, Burlingame, CA). SH-SY5Y cells, HEK293T cells and primary cultured dopaminergic neurons cultured in 4-well tissue culture chamber were fixed with 10% formaldehyde for 60 min on ice followed by acetone treatment for 5 min. They were then permeabilized with PBS containing 0.2% Triton X-100 for 10 min at room temperature and blocked with 10% goat serum for 30 min. They were then exposed to primary antibody overnight at 4 °C for indirect immunofluorescence. Anti-p38MAPK antibody and anti-p-p38MAPK were diluted 25-fold and 100-fold, respectively, with PBS containing 1% BSA before use. For immunofluorescence, primary antibodies were visualized by incubation for 2 h at room temperature with Alexa Fluor488- and Alexa Fluor546-conjugated secondary antibodies (Molecular Probes), followed by confocal laser scanning fluorescence microscopy using an LSM510 microscope(Carl Zeiss, Thornwood, NY).

TH-positive Cell and Ubiquitin-positive Inclusion Counting—Total numbers of TH-positive neurons in the substantia nigra pars compacta (SNc) and ubiquitin-positive inclusions in the striatum were determined using an unbiased optical fractionator method (Stereoinvestigator, MicroBrightField) as previously described with minor modification (4). Three independent sets of immunostained serial sections (sampled as every sixth coronal section throughout the entire range of SNc or the striatum) were analyzed for each animal. Total positive number for each sample was determined in triplicate by the Stereoinvestigator program to obtain averaged values. Location of SNc and the striatum was identified according to established anatomical landmarks (Paxinos mouse brain atlas).

Measurements of Striatal Catecholamines (HPLC)—Tissues dopamine and metabolites were measured according to previously published methods (4).

Plasmids, Cell Culture, Reagent, and Transfection—Various vectors, including pCMVfull-EGFP-ATF6α (also known as green fluorescent protein (GFP)-ATF6α fusion gene) (11), pGL3-GRP78 (−132)-Luc carrying the human BiP promoter, pGL3–5×UPRE-luc, pDNA3.1 (+)-N-terminal fragment of ATF6α (1–373) and a dominant-negative form of ATF6α (171–373) were prepared as previously (13, 14). Flag-p38MAPK was kindly provided by Dr. Katsuji Yoshioka (Kanazawa Univ.) ATF6α WT/KO primary cultured dopaminergic neurons were prepared as shown under "Primary culture." ATF6α WT/KO MEFs were obtained as previously described (7). SH-SY5Y cells were cultured in DMEM supplemented with 10% fetal bovine serum, NEAA (Invitrogen) at 37 °C in a humidified 5% CO_2/95% air atmosphere. HEK293T cells and ATF6α WT/KO MEFs were cultured in DMEM supplemented with 10% fetal bovine serum, 2 mM glutamine, and antibiotics (100 units/ml penicillin and 100 μg/ml streptomycin). Transfection was performed using Lipofectamine 2000 (Invitrogen, Carlsbad, CA) according to each manufacturer's protocol. 1-Methyl-4-phenylpyridinium iodide (MPP^+) was purchased from Sigma-Aldrich. SB203585 were purchased from Calbiochem (San Diego, CA). SHSY5Y cells and ATF6α WT/KO primary cultured dopaminergic neurons were treated with 1 mM MPP^+ for indicated times in the presence or absence of 5 μM SB203585. ATF6α WT/KO MEFs and HEK293T cells were plated in 6-well plates and treated with 50 μM hydroxyl peroxide (H_2O_2) (Nakalai Tesque, Kyoto) in the presence or absence of 5 μM SB203585.

Primary Culture—Mesencephalic and striatal cells were prepared from embryonic day 15 ATF6α WT/KO mice. Both the midbrain and the striatum were mechanically dissected in Neurobasal medium (Invitrogen). The tissues were dissociated with 0.25% trypsin at room temperature for 15 min. The cells were suspended in DMEM supplemented with 10% fetal bovine serum and NEAA and then collected by centrifugation (1000 × *g*, 3 min). The cells were resuspended in Neurobasal medium supplemented with B-27(minus Anti-Oxidants) (Invitrogen) and 0.5 mM glutamine at a concentration of 1million cells/ml, and plated at a density of 0.5 million cells per well into 24 well plate previously coated with poly-L-Lysin (Sigma-Aldrich). One week after plating, the cells were used for reporter assay or immunohistochemistry.

Reporter Assay—SH-SY5Y cells, HEK293T cells and ATF6α WT/KO primary cultured dopaminergic neurons were transiently transfected with pGL3–5×UPRE or pGL3-BiP (-132) along with pRL-SV40 (Promega, Madison, WI) using Lipofectamine 2000 (Invitrogen). After 48 h, the cells were treated with 1 mM MPP^+ for 24 h or 50 μM H_2O_2 for 1 h in the presence or absence of 5 μM SB203585. Luciferase expression was measured in triplicate using a dual luciferase reporter assay system (Promega) on Fluoroskan Ascent FL (Thermo, Waltham, MA). Relative activity was defined as the ratio firefly luciferase activity to *Renilla* luciferase activity to normalize for transfection efficiency.

Immunoprecipitation—After being washed with PBS, SH-SY5Y cells and HEK293T cells cultured in a 6-well plate dish were solubilized for 30 min on ice in 200 μl of RIPA buffer (50 mM Tris-HCl, 150 mM NaCl, 1 mM EDTA, 1% Triton X-100, 0.1% SDS, and 0.1% sodium deoxycholate) with a protease inhibitor mixture and a phosphatase inhibitor. Insoluble fraction was collected by centrifugation (1000 × *g*, 3 min), defined as nuclear fraction, and lysed in SDS lysis solution (50 mM Tris-HCl, 10 mM EDTA, 1% SDS) including phosphatase inhibitor. Soluble lysates were incubated overnight with ANTI-FLAG M2 Affinity gel (Sigma-Aldrich). Lysates from nuclear fraction were diluted to 10% by dilution buffer (50 mM Tris-HCl, 167 mM NaCl, 1.1% Triton X-100, and 0.11% sodium deoxycholate) including phosphatase inhibitor and then incubated for overnight by G-Sepharose bound to anti-phospho-p38MAPK antibody(Cell Signaling). Sepharose beads were collected by brief centrifugation and washed with TBS buffer (50 mM Tris-HCl, 150 mM NaCl, pH7.4) three times. Immunoprecipitated material was eluted by boiling for 3 min in 2× sample buffer (125 mM Tris-HCl, pH 6.8, 4% SDS, 20% glycerol, 0.004% BPB).

Chromatin Immunoprecipitation (ChIP) Assay—SH-SY5Y cells were grown to 80% confluence in 6-cm plates and then treated with 1 mM MPP^+ for 24 h and protein-DNA cross-linking was initiated by adding formaldehyde to the cell culture to a final concentration of 1% and stopped at 15 min by adding 1.5 M glycine to a final concentration of 0.15 M. The cells were lysed in RIPA buffer including a protease inhibitor mixture and a phosphatase inhibitor. Insoluble fraction was collected by centrifugation (1000 × *g*, 3 min), defined as nuclear fraction, lysed in SDS lysis solution (50 mM Tris-HCl, 10 mM EDTA, 1% SDS) including phosphatase inhibitor and sonicated for 25 min using Bioruptor (UCD-200TM, COSMO BIO) (Sonication pulse was performed by power high, ON 30 s, OFF 60 s). Diluted to 10% by ChIP dilution buffer (50 mM Tris-HCl, 167 mM NaCl, 1.1% Triton X-100, and 0.11% sodium deoxycholate) including phosphatase inhibitor, lysates were incubated for overnight by G-Sepharose bound to anti-phospho-p38MAPK antibody. Sepharose beads were collected by brief centrifugation, washed with RIPA buffer three times and suspended with ChIP direct elution buffer (10 mM Tris-HCl, 300 mM NaCl, 5 mM EDTA, 0.5% SDS). Formaldehyde-induced cross linking was reversed (for overnight at 65 °C) and the DNA was purified by phenol-chloroform extraction and ethanol precipitation. Purified DNA was subjected to quantitative PCR by LightCycler 480 program.

Statistical Analysis—All values are presented as the mean ± S.D. Results were tested for significant differences using one-way ANOVA with the posthoc test or Student's *t* test. $p < 0.05$ was considered to represent significant difference. In figures, a single asterisk (*) indicates $p < 0.05$, and a double asterisk (**) indicates $p < 0.01$.

RESULTS

ATF6α Controls the Levels of ER Chaperones and ERAD Component in the Dopaminergic Neuron System in Vivo—To explore the physiological function of ATF6α *in vivo*, we first investigated where in the central nervous system ATF6α is

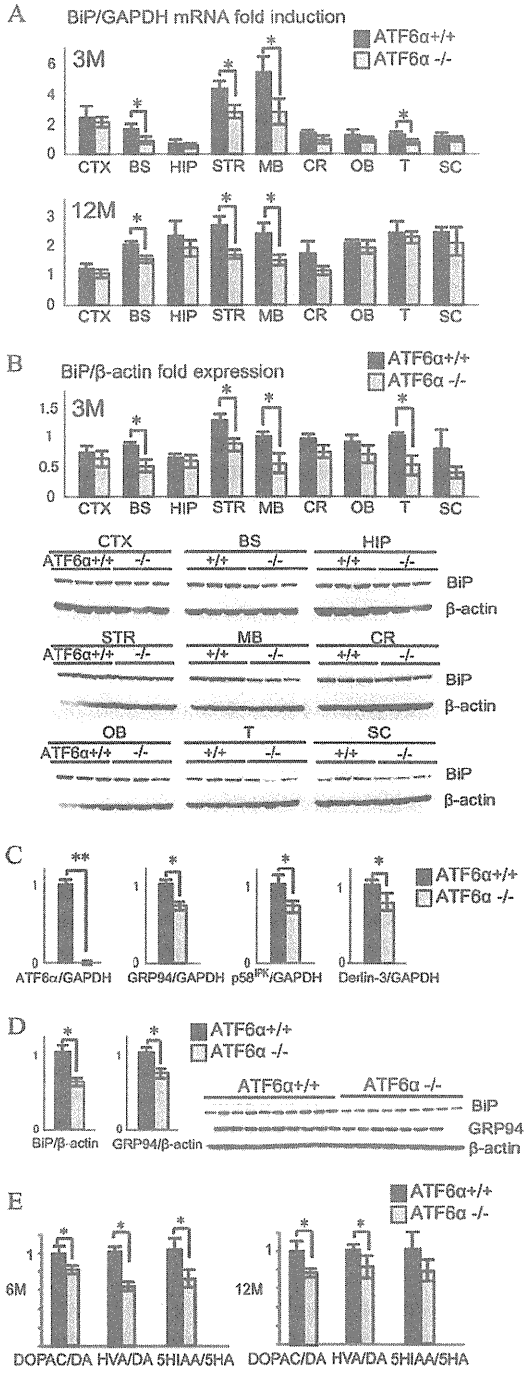

FIGURE 1. **ATF6α controls the levels of ER chaperones and ERAD component in the dopaminergic neuron system under physiological conditions *in vivo*.** *A*, ATF6α controls the mRNA levels of BiP in the brainstem, the midbrain and the striatum in mice brain *in vivo*. Total RNA was isolated from various sections of brain of 3 and 12-month-aged male ATF6α KO(−/−) mice and ATF6α WT(+/+) littermates and analyzed by quantitative real-time RT-PCR for detecting the level of BiP mRNA. ($n = 5$ for each group). Fold induction of mRNA level is defined relative to GAPDH mRNA level. Abbreviation: *CTX*, cerebral cortex; *BS*, brainstem; *HIP*, hippocampus; *STR*, striatum; *MB*, midbrain; *CR*, cerebellum; *OB*, olfactory bulb; *T*, thalamus; *SC*, spinal cord; 3 M, 3 months aged group; 12 M, 12-month-aged group. The *asterisk* indicates statistical significance (*, $p < 0.05$; **, $p < 0.01$). Each bar denotes the mean ± S.D. *B*, ATF6α controls the protein levels of BiP in the brainstem, the midbrain and the striatum in mice brain *in vivo*. The tissue lysates of 3-month-aged ATF6α KO mice and ATF6α WT littermate were subjected to Western blot analysis for detection of BiP and β-actin ($n = 5$). Each protein level was quantified using optical density and estimated relative to β-actin protein level. *C*, ATF6α controls the levels of GRP94, p58^{IPK}, and Derlin-3 in the midbrain *in vivo*. Quantitative real-time RT-PCR was performed from the midbrain samples of 12-month-aged ATF6α KO mice and ATF6α WT littermates using ATF6α, GRP94, p58^{IPK}, and Derlin-3 primers ($n = 5$ for each group). *D*, ATF6α controls the protein levels of BiP and GRP94 in the striatum *in vivo*. ($n = 7–10$). *E*, metabolisms of dopamine and serotonin were decreased in ATF6α KO mice as compared with ATF6α WT mice. Metabolisms of dopamine and serotonin were defined as the relative ratio of DOPAC or HVA to dopamine and 5HIAA to 5HA, respectively. The striatal levels of dopamine, serotonin, and their metabolites were measured by HPLC ($n = 8–10$ for each group). Abbreviations: *DA*, dopamine; *DOPAC*, 3,4-dihydroxyphenylacetic acid; *HVA*, homovanillic acid; *5HIAA*, 5-hydroxyindole acetic acid; *5HA*, 5-hydroxytryptamine; 6 M, 6-month-aged group; 12 M, 12-month-aged group.

activated under normal physiological conditions by using ATF6α WT or KO mice. Results of quantitative RT-PCR analysis demonstrated that mRNA level of the ER chaperone BiP was significantly lower in the brainstem, the midbrain and the striatum of ATF6α KO mice than those of ATF6α WT mice (Fig. 1*A*). Accordingly, the protein levels of BiP were also significantly lower in the brainstem, the midbrain and the striatum of ATF6α KO mice than those of ATF6α WT mice (Fig. 1*B*). Other ER stress sensor, IRE1α, sXBP1, and phosphorylated PERK (p-PERK, indicative of the activation status of another ER stress sensor molecule) are not different in various brain regions of ATF6α KO mice (supplemental Fig. S1*A*). The mRNA levels of other ER chaperone GRP94, cochaperone p58^{IPK}, and ERAD component, Derlin-3, in the midbrain were also significantly decreased in ATF6α KO mice when compared with age-matched ATF6α WT mice (Fig. 1*C*). The protein levels of GRP94 in the striatum were significantly decreased in ATF6α KO mice (Fig. 1*D*). HPLC analysis of the striatum demonstrated that the metabolisms of dopamine and serotonin were slightly but significantly decreased in ATF6α KO mice as compared with WT mice (Fig. 1*E*). Decreased protein levels were not general feature of ATF6α KO mice because the levels of some proteins involved in synaptic secretion or vesicular transport remained unchanged or rather increased in ATF6α KO mice as compared with WT mice (supplemental Fig. S1*B*). Importantly, tyrosine hydroxylase (TH) immunostaining of the midbrain revealed that there was no abnormality in the number and morphology of TH positive neurons in ATF6α KO mice when compared with WT littermates (supplemental Fig. S1, *C* and *D*). TH and DAT protein levels in the striatum of ATF6α KO mice were similar to those of WT littermates (supplemental Fig. S1*E*). Therefore, although ATF6α is not essential for the development and the survival of dopaminergic neurons, ATF6α up-regulates ER chaperones and ERAD component constitutively in dopaminergic neurons; dopaminergic neurons may experience ER stress under normal physiological conditions.

MPTP Up-regulates the Levels of ER Chaperones and ERAD Component by Activating ATF6α and Induces the Phosphorylation of p38MAPK in the Dopaminergic Neurons in Vivo—To investigate whether ATF6α plays an important role in dopaminergic cell death of neurotoxin-based PD models, we analyzed dopaminergic neurons of mice treated with MPTP. MPTP was intraperitoneally administered into 6-month-old

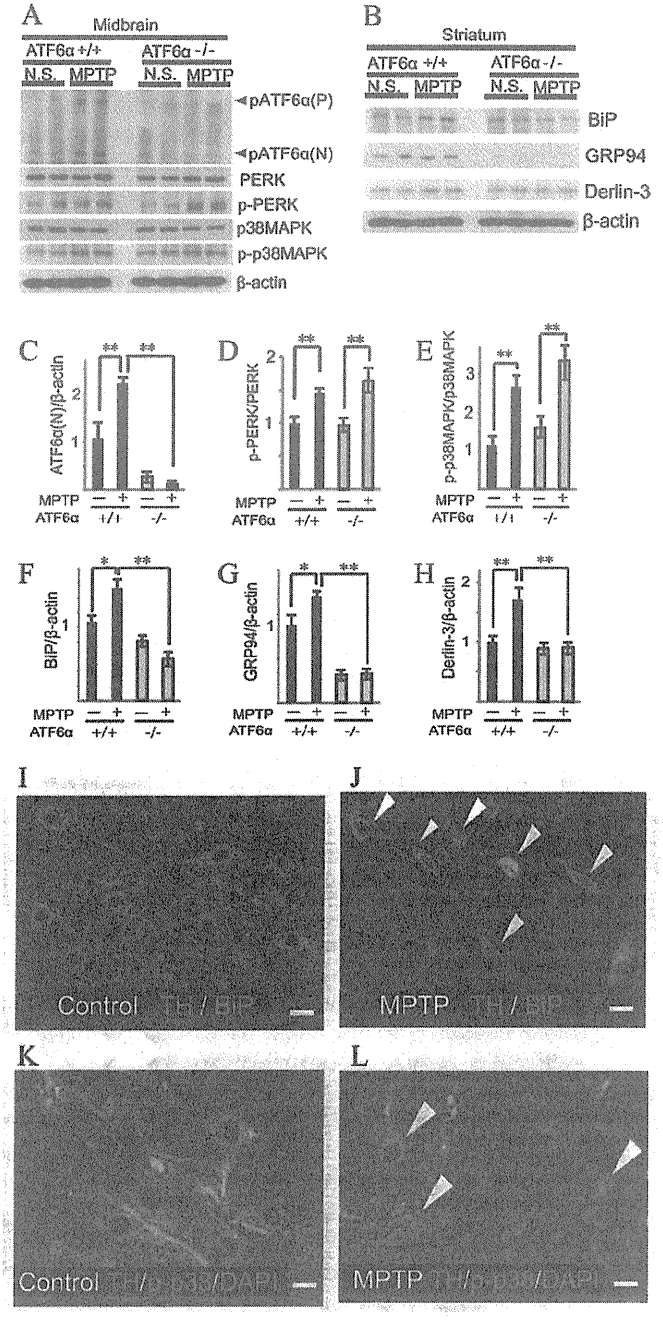

FIGURE 2. MPTP up-regulates the levels of ER chaperones and ERAD component by activating ATF6α and induces the phosphorylation of p38 MAPK in dopaminergic neurons *in vivo*. *A–H*, extracts of the midbrain or the striatum of ATF6α WT(+/+) and ATF6α KO(−/−) mice were prepared 5 days after intraperitoneal injection with either 20 mg/kg MPTP or normal saline four times every 2 h for Western blot analysis of ATF6α, PERK, p38MAPK, phospho-PERK (p-PERK), phospho-p38MAPK (p-p38MAPK), BiP, GRP94, Derlin-3, and β-actin ($n = 4$ for each group). The protein levels of p-PERK and p-p38MAPK were quantified using optical density and estimated relative to PERK or p38MAPK protein level, respectively. Other protein levels were estimated relative to β-actin protein level. Each bar denotes the mean ± S.D. MPTP induces ATF6α cleavage (*A* and *C*), phosphorylation of PERK (*A* and *D*) and p38MAPK activation (*A* and *E*) in the midbrain. MPTP up-regulates the levels of BiP (*B* and *F*), GRP94 (*B* and *G*), and Derlin-3 (*B* and *H*) in the striatum *in vivo*. Abbreviation: *N.S.* indicates normal saline injection as control. *I–L*, MPTP up-regulates the levels of BiP and p-p38MAPK in TH-positive neurons. The midbrains of ATF6α WT mice treated with MPTP or normal saline (Control) were stained using anti-TH (*I–L*, *green*), BiP (*I* and *J*, *red*), p-p38MAPK (*K* and *L*, *red*) antibodies, and DAPI (*K* and *L*, *blue*). They were visualized by Alexa Fluor 488- and Alexa Fluor 546-conjugated secondary antibodies and subjected to confocal fluorescence microscope analysis. *White arrowheads* in *J* and *L* indicate the TH-positive dopaminergic cells of MPTP-treated mice. Scale bars indicate 10 μm.

ATF6α KO mice and WT littermates. Western blot analysis with antibodies against ATF6α, PERK, p38MAPK, phosphorylated p38MAPK (p-p38MAPK), p-PERK, BiP, GRP94, and Derlin-3 was performed using midbrain and striatal extracts from WT or ATF6α KO mice challenged with MPTP. MPTP treatment induced phosphorylation of p38MAPK in the midbrain regardless of ATF6α genotype as expected (Fig. 2, *A* and *E*). Importantly, MPTP treatment not only increased the level of pATF6α (P), the precursor form of ATF6α, but also generated pATF6α (N), the active form produced as a result of the cleavage of pATF6α (P), in the midbrain of ATF6α WT mice (Fig. 2, *A* and *C*). The levels of ER chaperones, BiP and GPR94, and ERAD component, Derlin-3, were significantly increased in the striatum of MPTP-treated WT mice (Fig. 2, *B*, *F*, *G*, and *H*). In marked contrast, the induction of these ER chaperones and ERAD components was not observed in ATF6α KO mice even though MPTP increased phosphorylation of PERK regardless of ATF6α genotype (Fig. 2, *A* and *D*). To identify the cell types in which BiP was up-regulated, we performed double immunostaining for BiP in TH-positive dopaminergic neurons of the midbrain of WT mice. Dopaminergic neurons showed higher BiP expression level in MPTP-treated WT mice than untreated control mice (Fig. 2, *I* and *J*). Phosphorylated p38MAPK was detected in the nucleus of the dopaminergic neurons in the midbrain of MPTP-treated mice (Fig. 2, *K* and *L*) as previously reported (18). These data clearly indicate that MPTP somehow evokes ER stress and up-regulates the expression of ER chaperones and ERAD component by activating ATF6α in dopaminergic neurons *in vivo* in addition to previously known effect on the phosphorylation of p38MAPK. One possible cause for induction of ER stress by MPTP is production of ROS as we found that treatment of mouse embryonic fibroblasts (MEFs) derived from ATF6α WT mice with hydrogen peroxide, a representative ROS, triggered not only phosphorylation of p38MAPK but also cleavage of pATF6α(P) to produce pATF6α(N) (supplemental Fig. S2*A*).

ATF6α Protects against MPTP-induced Neurotoxicity in Vivo—We then asked whether ATF6α deletion and the sequential decline in the expression levels of ER chaperones and ERAD component have an impact on the ubiquitin proteasome system (UPS)-mediated protein degradation in dopaminergic neurons after MPTP treatment. Immunostaining of the striatum with antibody to ubiquitin revealed no difference in the striatum between ATF6α WT and KO mice under physiological conditions. However, upon stress with MPTP, the striatum of ATF6α KO mice showed much higher increase in the formation of clusters of ubiquitin-immunoreactive material than WT mice, suggesting that treatment with MPTP disturbed UPS more profoundly when the levels of ER chaperones and ERAD components were mitigated (Fig. 3, *A* and *B*). Next we assessed for neurotoxicity caused by treat-

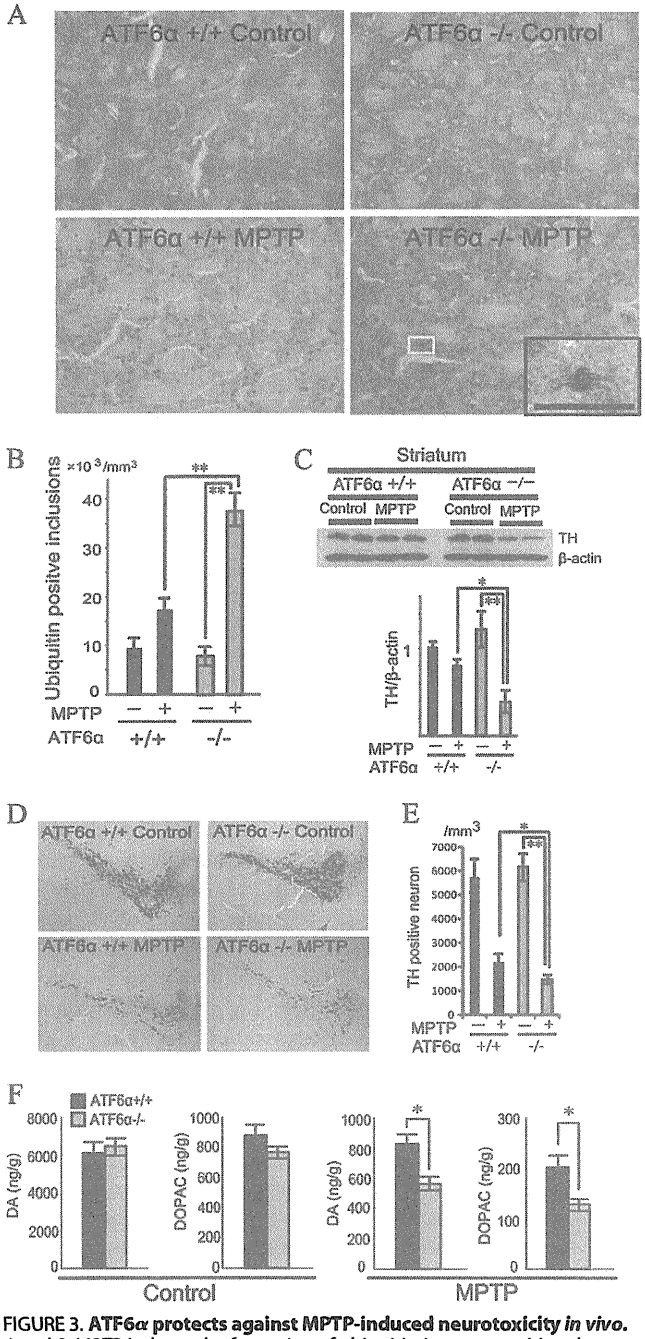

FIGURE 3. **ATF6α protects against MPTP-induced neurotoxicity *in vivo*.** *A* and *B*, MPTP induces the formation of ubiquitin-immunopositive clusters in the striatum of ATF6α KO(−/−) mice. *A*, representative images of ubiquitin-immunoreactive clusters in the striatum of ATF6α WT(+/+) and ATF6α KO mice treated with either 20 mg/kg MPTP or normal saline (Control) four times every 2 h. The *white box* marks the area enlarged in *lower right black box*. Scale bars indicate 50 μm. *B*, numbers of ubiquitin-immunoreactive inclusion per the volume of ROI in the striatum of individual mice were quantified by Stereoinvestigator and the density was compared among each indicated group. ($n = 4$ for each group). Each bar denotes the mean ± S.D. *C–F*, dopaminergic neurons of ATF6α KO mice are more vulnerable to MPTP neurotoxicity than ATF6α WT mice. *C*, extracts of the striatum of ATF6α WT and ATF6α KO mice with MPTP treatment or normal saline (Control) were subjected for Western blot analysis of TH and β-actin ($n = 4$ for each group). TH protein level was quantified using optical density and estimated relative to β-actin protein level. *D*, representative TH-immunostained images of the midbrain of ATF6α WT and ATF6α KO mice treated with normal saline (Control) or MPTP. *E*, TH-positive numbers in the midbrain SNc of ATF6α WT and ATF6α KO male littermates treated with MPTP or normal saline ($n = 5$ for each group). *F*, quantification of the striatal levels of dopamine and its metabolite DOPAC in ATF6α WT and ATF6α KO mice treated with either MPTP or normal saline (Control) ($n = 5$ for each group). Abbreviations: *DA*, dopamine; *DOPAC*, 3,4-dihydroxyphenylacetic acid.

ment with MPTP. Immunoblotting of the extracts from the striatum using TH antibody showed more remarkably decreased level of TH in ATF6α KO mice than in WT after treatment with MPTP, indicating that more dopaminergic terminal loss takes occurs in ATF6α KO mice (Fig. 3*C*). The number of TH-positive neurons in the SNc was significantly decreased in MPTP-treated ATF6α KO mice when compared with WT littermates (Fig. 3, *D* and *E*). These results were correlated with those of HPLC analysis, which showed significant decreases of dopamine and its metabolites, 3,4-dihydroxyphenylacetic acid (DOPAC), in the striatum of MPTP-treated ATF6α KO mice when compared with WT littermates (Fig. 3*F*). These results indicate that MPTP induces a larger loss of dopaminergic neurons and their terminals under ATF6α-deleted conditions and further suggest that ATF6α protects against MPTP-induced neurotoxicity.

Phosphorylated p38MAPK and Activated ATF6α Cooperate to Enhance the Expression Level of BiP in Dopaminergic Neurons Treated with MPP⁺—Next we investigated the possible cooperation between p38MAPK phosphorylated and ATF6α activated in MPTP-treated dopaminergic neurons. We treated dopaminergic neuroblastoma SH-SY5Y cells with MPP^+. Immunoblotting revealed that treatment with MPP^+ generated a ~60-kDa protein band representing pATF6α (N) (Fig. 4, *A* and *B*) and induced phosphorylation of PERK (Fig. 4, *A* and *C*) as well as that of p38MAPK (Fig. 4, *A* and *D*) in SH-SY5Y cells as in the midbrain of ATF6α WT mice (see Fig. 2*A*). SB203585, an inhibitor of p38MAPK phosphorylation, attenuated p38MAPK phosphorylation induced by MPP^+ (Fig. 4, *A* and *D*) but showed little effect on the activation of ATF6α and PERK phosphorylation (Fig. 4, *A–C*). We confirmed that SB203585 attenuated p38MAPK phosphorylation without affecting cleavage of pATF6α (P) in MEFs treated with hydrogen peroxide (supplemental Fig. S2*A*). However, BiP was up-regulated after MPP^+ treatment and this up-regulation was significantly reduced by SB203585 in SH-SY5Y cells (Fig. 4, *A* and *E*). This observation was further confirmed by BiP promoter-luciferase reporter system (Fig. 4, *F* and *G*). The reporter gene −132/LUC contains a fragment of the BiP promoter driving the luciferase expression. We introduced the BiP promoter-luciferase plasmid into SH-SY5Y cells with or without p38MAPK overexpression vector, and then treated transfected cells with MPP^+. Luciferase expression level continuously increased for 24 h after MPP^+ treatment and this MPP^+-induced stimulation of reporter expression was synergistically enhanced by p38MAPK overexpression (Fig. 4*F*). We then examined the effect of MPP^+ and SB203585 on reporter expression in the primary co-culture of the midbrain and the striatum prepared from ATF6α KO or WT mice (supplemental Fig. 2*C*). We found that MPP^+ treatment induced a significant increment in luciferase expression in cells from ATF6α WT and that this effect was abrogated by the presence

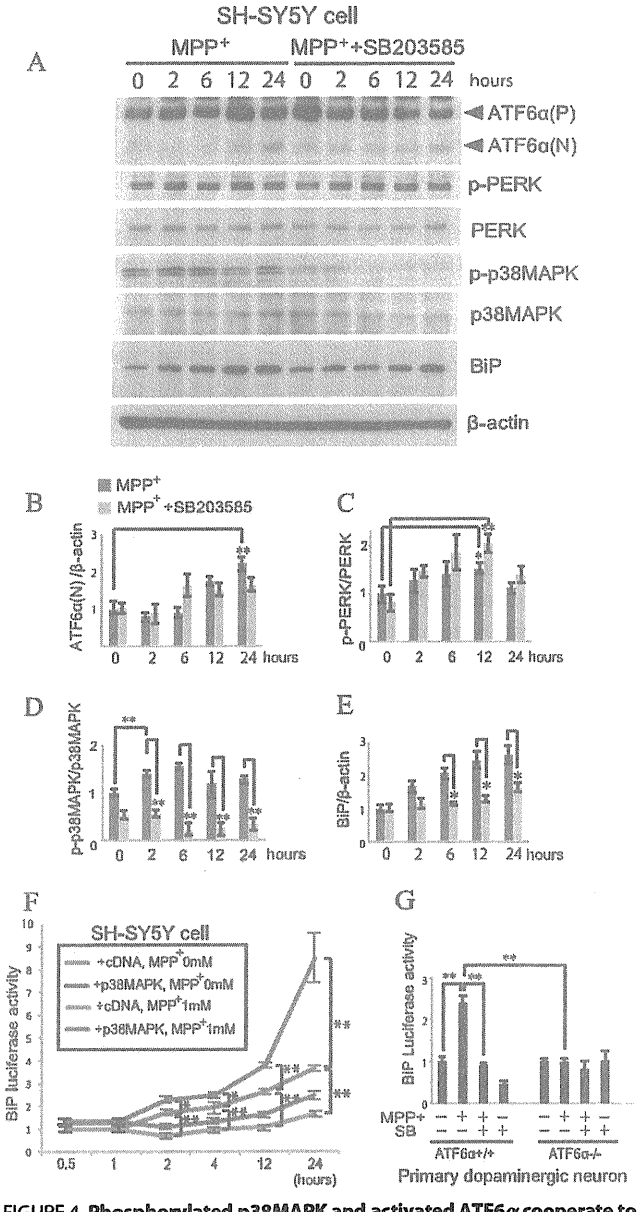

FIGURE 4. **Phosphorylated p38MAPK and activated ATF6α cooperate to enhance the expression level of BiP in dopaminergic neurons treated with MPP+.** *A–E*, immunoblot of cell lysates from SH-SY5Y cells treated with 1 mM MPP^+ for 2, 6, 12, 24 h using anti-ATF6α, phosphorylated PERK (p-PERK), PERK, p38MAPK, phosphorylated p38MAPK (p-p38MAPK), BiP, and β-actin antibodies. 5 μM SB203585 was added into the medium prior to MPP^+ treatment for the indicated times. Densitometry of ATF6α (N) (*B*), p-PERK (*C*), p-p38MAPK (*D*), and BiP (*E*) was performed on scanned *immunoblots* images using the *Image-J and* normalized to β-actin, PERK, p38MAPK, and β-actin, respectively. Each bar denotes the mean ± S.D. *F*, BiP promoter-Luciferase plasmid and pRL-SV40 plasmid were transfected into SH-SY5Y cells with p38MAPK overexpression vector or Mock vector. Each group of transfected cells was treated with or without 1 mM MPP^+ for 0.5, 1, 2, 4, 12, 24 h. Relative activity is defined as the ratio of firefly luciferase activity to *Renilla* luciferase activity in dual-luciferase assay. *G*, dopaminergic neurons from primary co-culture of the midbrain and the striatum of ATF6α WT(+/+) or ATF6α KO(−/−) mice transfected with BiP promoter-Luciferase vector and pRL-SV40 vector and then treated with 1 mM MPP^+ for 24 h with or without 5 μM SB203585. Relative activity is defined as the ratio of firefly luciferase activity to *Renilla* luciferase activity in dual-luciferase assay.

of SB203585 (Fig. 4*G*). In contrast, reporter expression remained unchanged in MPP^+-treated cells derived from ATF6α KO. These data suggest that phosphorylation of p38MAPK induced by treatment with MPP^+ positively affects the ATF6α-mediated transcriptional induction of BiP.

MPP^+ Induces the Translocation of the N-terminal Fragment of ATF6α to the Nucleus and the Binding of N-terminal ATF6α with Phosphorylated p38MAPK and Enhances the Transcriptional Activity of ATF6α—To examine possible interaction between ATF6α and p38MAPK, we conducted immunofluorescence analysis of primary cultured dopaminergic neurons transfected with vectors to express green fluorescent protein (GFP) fused to the N terminus of full-length ATF6α (pGFP-ATF6α(P)), which is cleaved to produce nuclear-translocating pGFP-ATF6α(N) in response to ER stress (11), using anti-phosphorylated p38MAPK (p-p38MAPK) or anti-p38MAPK antibodies. GFP-ATF6α (P) was localized in the peri-nuclear region in non-stressed dopaminergic neurons (Fig. 5*A*) and was partially colocalized with cytosolic p38MAPK (Fig. 5*B*) in non-stressed dopaminergic neurons. 24 h after the treatment with MPP^+, pGFP-ATF6α (N) was translocated into the nucleus and colocalized with both DAPI and p-p38MAPK (Fig. 5*C*). By treating SH-SY5Y cells with MPP^+ after expression with both pGFP-ATF6α (P) and p38MAPK we confirmed that pGFP-ATF6α (N) was translocated into the nucleus and colocalized with both DAPI and p-p38MAPK (supplemental Fig. S3, *A–C*). To determine whether ATF6α physically associates with p-p38MAPK, we cotransfected flag-p38MAPK vector and the N-terminal fragment of ATF6α vector (1–373), abbreviated to N-ATF6α, into SH-SY5Y cells and performed immunoprecipitation with an anti-Flag antibody followed by immunoblotting with anti-ATF6α antibody. As shown in Fig. 5*D* (*upper panel*), pATF6α (N) (60kDa) and pATF6α (P) (90 kDa) were detected in the immunoprecipitates after treatment of MPP^+. SB203585 attenuated the intensity of both bands in immunoprecipitates from MPP^+-treated SH-SY5Y cells. Both pATF6α (N) (60 kDa) and pATF6α (P) (90 kDa) were also increased in the nuclear fraction of MPP^+-treated SH-SY5Y lysates after immunoprecipitation with anti-p-p38MAPK antibody as shown in Fig. 5*D* (*middle panel*). Endogenous N-ATF6α can bind to p-p38MAPK in MPP^+-treated condition and this binding was attenuated by adding SB203585 (Fig. 5*E*). Next we examined whether the p-p38MAPK-ATF6α complex binds to the promoter region of BiP in the nuclear fraction using ChIP assay. As shown in Fig. 5*F*, SH-SY5Y cells were treated with MPP^+ for 24 h and then cross-linked with formaldehyde. Extracted nuclear fraction was subjected to immunoprecipitation with p-p38MAPK antibody. Fragmented genomic DNA was extracted from the immunoprecipitates and quantified by QPCR using the primers for ERSEs of BiP promoter regions (−155~−21). MPP^+ enhanced the binding p-p38MAPK-ATF6α complex to ERSEs, which was reduced by p38MAPK inhibitor (Fig. 5, *G* and *H*). We amplified the other cis-elements on Neurogenin2 (a neural basic-loop-helix (bHLH) transcriptional factor, Ngn2) promoter using the genomic DNA extracted

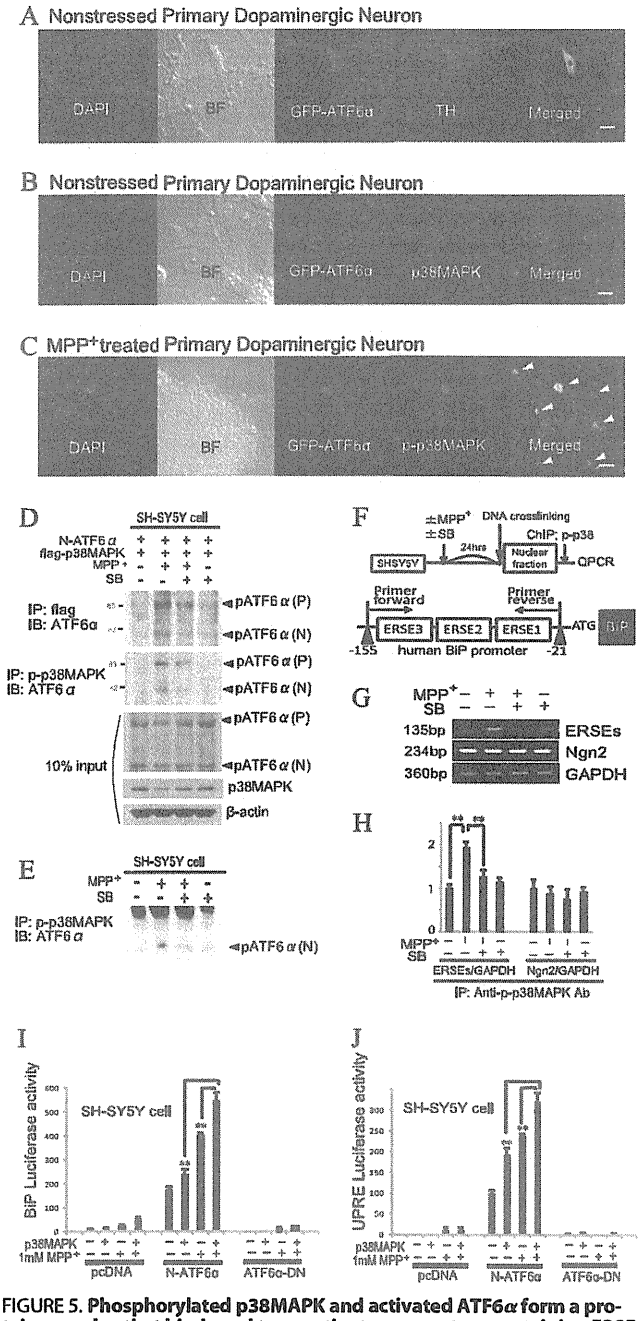

FIGURE 5. **Phosphorylated p38MAPK and activated ATF6α form a protein complex that binds and transactivates promoters containing ERSE and UPRE.** *A–C*, MPP^+ induces release of N-terminal ATF6α fragment with subsequent translocation into the nucleus and colocalization with phosphorylated p38MAPK in dopaminergic neurons. 24 h after transfection with pGFP-ATF6α (P), primary cultured dopaminergic neurons from co-culture of the midbrain and the striatum of ATF6α KO mice were fixed and stained with anti-TH antibody (*A*, *red*), anti-p38MAPK antibody (*B*, *red*), and DAPI (*blue*). 24 h after transfection with pGFP-ATF6α (P), primary cultured dopaminergic neurons were treated with 1 mM MPP^+ for 24 h, and then fixed for staining with phosphorylated p38MAPK (p-p38MAPK) antibody (*C*, *red*) and DAPI (*blue*). *White arrowheads* indicate the nuclear localization of DAPI, GFP, and p-p38MAPK. Scale bars indicate 10 μm. Abbreviations: *TH*, tyrosine hydroxylase; *BF*, bright-field image. *D–H*, MPP^+ treatment induces the binding among p-p38MAPK, N-terminal fragment of ATF6α and ERSEs of BiP promoter regions. SH-SY5Y cells were transfected with Flag-p38MAPK vector and N-terminal fragment of ATF6α-(1–373) vector. They were then cultured with or without 1 mM MPP^+ in the presence or absence of 5 μM SB203585 for 24 h. Cells were lysed in RIPA buffer and separated into soluble or insoluble fraction. *D*, soluble fraction was immunoprecipitated with anti-Flag antibody and immunoblotted with anti-ATF6α antibody (*upper panel*). Insoluble fraction was immunoprecipitated with anti-p-p38MAPK antibody and immunoblotted with anti-ATF6α antibody (*middle panel*). Western blot analysis of 10% input of soluble fraction was performed with anti-ATF6α, p38MAPK and β-actin antibodies (*lower panels*). Abbreviations: *IP*, immunoprecipitation; *IB*, immunoblotting; *SB*, SB203585; *N-ATF6α*, N-terminal fragment of ATF6α-(1–373). *E*, endogenous N-terminal fragment of ATF6α can bind to phosphorylated p38MAPK in MPP^+-treated condition. SHSY5Y cells were cultured without transfection and treated with or without 1 mM MPP^+ in the presence or absence of 5 μM SB203585 for 24 h. Cells were totally lysed in RIPA buffer using BIORUPTOR and immunoprecipitated with anti-p-p38MAPK antibody and immunoblotted with anti-ATF6α antibody. *F*, P-p38MAPK-ATF6α complex binds to ERSEs in response to MPP^+ treatment. *Upper panel* shows schematic representation of ChIP assays. SH-SY5Y cells were treated with or without MPP^+ in the presence or absence of 5 μM SB203585 for 24 h and then cross-linked with formaldehyde. Cells were lysed in RIPA buffer, and the insoluble fraction defined as nuclear fraction was lysed in SDS buffer. Immunoprecipitated with anti-p-p38MAPK, purified, and input DNAs were analyzed by Quantitative PCR using the primers shown in lower panel. *G*, primers used for human endogenous BiP promoter, Neurogenin2 (Ngn2) promoter and GAPDH yielded 135, 234, and 360 bp PCR products, respectively. *H*, values of PCR products were measured by QPCR and fold induction was defined as the value of BiP or Ngn2 promoter regions relative to the value of GAPDH. Each bar denotes the mean ± S.D. *I* and *J*, p38MAPK phosphorylation enhances the transcriptional activity of ATF6α. *I*, vectors(1 μg of BiP promoter-Luciferase vector, 100 ng of pRL-SV40 vector and 1 μg of control vector or p38MAPK vector) were mixed with 1 μg of Mock(pcDNA-3.1(+)) or N-terminal fragment (1–373)(N-ATF6α) or dominant-negative form (171–373) of ATF6α vector (ATF6α-DN) for transfection of SH-SY5Y cells in a 6-well dish for 48 h. Cells were challenged with or without 1 mM MPP^+ for 24 h and lysed for analysis of BiP reporter expression. *J*, vectors (1 μg 5 × UPRE reporter vector, 100 ng pRL-SV40 vector and 1 μg of control vector or p38MAPK vector) were mixed with 1 μg of pcDNA-3.1(+) or N-ATF6α or ATF6α-DN vector for transfection of SH-SY5Y cells in a 6-well dish for 48 h. Cells were challenged with or without 1 mM MPP^+ for 24 h and lysed for analysis of UPRE reporter expression.

We finally investigated whether the expression of p38MAPK and/or the treatment with MPP^+ could increase the transcriptional activity of nuclear-translocating ATF6α using the BiP promoter-luciferase system. MPP^+ was added to SH-SY5Y cells cotransfected with Mock or N-ATF6α encoding transactivator domain (TAD) and the DNA-binding b-ZiP domain or the dominant-negative form lacking TAD of ATF6α (ATF6α-DN) in the presence or absence of p38MAPK. MPP^+ treatment significantly enhanced the stimulative effect of p38MAPK on N-ATF6α-mediated activation of BiP reporter expression (Fig. 5*I*). We also found that MPP^+ treatment increased transcriptional activator activity of N-ATF6α through UPRE, which has been shown to be present in the promoter region of ERAD components and be functional in the induction of ERAD components (22, 23), and further enhanced it in presence of p38MAPK (Fig. 5*J*). ATF6α-DN canceled these enhancement induced by p38MAPK overexpression through ERSE and UPRE. Thus, MPP^+ promotes phosphorylation of p38MAPK and the binding with the N-terminal ATF6α, leading to up-regulation of ATF6α transcriptional activity.

Hydrogen peroxide also induced the translocation of the N-terminal fragment of ATF6α into the nucleus, where it co-localizes with p-p38MAPK (supplemental Fig. S3, *D–G*). Hydrogen peroxide promoted the binding of N-ATF6α with phosphorylated p38MAPK and enhanced the transcriptional activity of N-ATF6α through ERSE and UPRE (supplemental Fig. S3, *H–J*).

DISCUSSION

In this study, we concluded that ATF6α plays an important role in protection from MPTP toxicity in the dopaminergic neurons via up-regulation of ER chaperones and ERAD component. This was based on the following findings: 1) ATF6α controls the levels of ER chaperones and ERAD component in dopaminergic neurons-containing brain regions (Figs. 1, *A–D*) and 2). Both MPTP and MPP^+ upregulate the expression levels of ER chaperones and ERAD component by activating ATF6α in dopaminergic neurons and SH-SY5Y cells (Fig. 2, *A, B, C, F, G, H* and 4, *A, B, E, F,* and *G*); 3) MPTP triggers more formation of clusters of ubiquitin-immunoreactive material in the striatum of ATF6α KO mice than in WT mice (Fig. 3, *A* and *B*); 4) Dopaminergic neurons under ATF6α KO conditions are more vulnerable to MPTP neurotoxicity (Fig. 3, *C–F*). Previous studies showed that MPTP and 6-OHDA induce various ER stress mediators *in vitro* (24–26). However, it has been unclear how these neurotoxins induce UPR.

A plausible mechanism is that MPTP decreases the protein degradation function of striatal UPS (27). A single or intermittent dose of MPTP decreases UPS activity only for a short time and does not lead to the ubiquitinated inclusion bodies in rodent brain (28). In contrast, continuous MPTP administration causes long-lasting impairment of UPS and the production of inclusion bodies immunoreactive for ubiquitin and α-synuclein in the rodent SNc (27). This report suggests that the inhibition of UPS by MPTP causes the accumulation of unfolded proteins followed by activation of UPR, finally leading to ER stress-induced cell death.

Consistent with this hypothesis, our study demonstrated that UPR attenuation caused by ATF6α deletion accelerates the MPTP-induced formation of ubiquitin immunopositive inclusion body in the striatum as well as dopaminergic neuronal death (Fig. 3). This result suggests that MPTP induces accumulation of ubiquitin-positive aggregates presumably as a result of oxidative protein damage to protein folding and its machineries (29–31) and that activated ATF6α promotes refolding and/or elimination of ubiquitinated proteins in the nerve terminal of dopaminergic neuron by the action of induced ER chaperones and ERAD components. These findings strongly suggest that both UPS and UPR are involved in MPTP-induced dopaminergic neuronal depletion. In our study we stained the striatal sections from MPTP-treated ATF6α WT and KO mice with thioflavin T (amyloid-specific dye) and immunostained with anti-α-synuclein antibody and anti-phosphorylated α-synuclein. However we could not detect any stained aggregates for them (supplemental Fig. S2*B*). Although it remains to be elucidated what is the major component of the ubiquitinated aggregates in this study, we speculates that oxidative products should be ubiquitinated and accumulated after oxidative stress induced by MPTP.

MPP^+ interferes with the mitochondrial complex-1, generates ROS. ROS are also generated in the degradation process of dopamine and therefore dopamine is the most oxidative neurotransmitter in brain (16). In the present study, ATF6α was activated particularly in the dopaminergic neuron system (Fig. 1, *A* and *B*) and the metabolism of dopamine is decreased in ATF6α KO mice (Fig. 1*E*), suggesting that ROS generated from dopamine metabolic process may play a critical role in the up-regulation of ATF6α-mediated UPR.

Previous study showed that ROS induced by both MPP^+ and dopamine metabolism promotes phosphorylation of p38MAPK (17, 18, 32). Phosphorylated p38MAPK phosphorylates ATF6α and mediates the transcriptional induction of the atrial natriuretic factor gene through a serum response element (21, 33). To explore the relationship between oxidative stress by ROS and UPR by ATF6α, we focused on p38MAPK.

We demonstrated that: 1) Both MPTP and MPP^+ induce the phosphorylation of p38MAPK in dopaminergic neurons as well as in SH-SY5Y cells (Figs. 2, *A, E, K, L* and 4, *A* and *D*). 2) MPP^+ induces ATF6α-mediated up-regulation of BiP expression level in a p38MAPK-dependent manner (Fig. 4, *A, E, F,* and *G*). 3) MPP^+ triggers the translocation of N-terminal ATF6α to the nucleus and the binding of N-terminal ATF6α with phosphorylated p38MAPK to enhance the transcriptional activity of ATF6α in dopaminergic neurons (Fig. 5, *C–J*). Hydrogen peroxide, a representative ROS, also activated ATF6α and phosphorylated p38MAPK (supplemental Fig. S2*A*). Hydrogen peroxide promoted the formation of N-ATF6α-p-p38MAPK complex and enhanced the transcriptional activity of ATF6α to up-regulate ER chaperones and ERAD components (supplemental Fig. S3, *D–J*).

Based on these data, we propose that MPP^+-derived oxidative stress results in phosphorylation of p38MAPK, enhancement of ATF6α transcriptional activity, induction of ER chaperones and ERAD components and degradation of ubiquitinated accumulated proteins in dopaminergic neurons. In contrast, under ATF6α-deleted condition, MPP^+ triggers the formation of ubiquitinated aggregates in the striatum, and this protein accumulation lead to apoptosis of the dopaminergic neurons (Fig. 6).

ER stress and oxidative stress are closely linked events. Another oxidative neurotoxin, 6-OHDA, causes rapid generation of ROS, oxidative modification of protein and activates UPR. Antioxidants reduce UPR activation and apoptosis, and improve protein secretion (29). This study suggests that UPR protects against oxidative stress-induced cell death. ER stress preconditioning of BiP attenuates H_2O_2-induced cell injury in LLC-PK1 cells (34). Precondition of ER chaperones in the striatum expressed by ATF6α under physiological conditions may also suppress dopaminergic neurons depletion induced by MPP+-derived oxidative stress.

The p38MAPK pathway is stimulated by cellular stresses, such as free radicals and inflammatory agents, and mediates

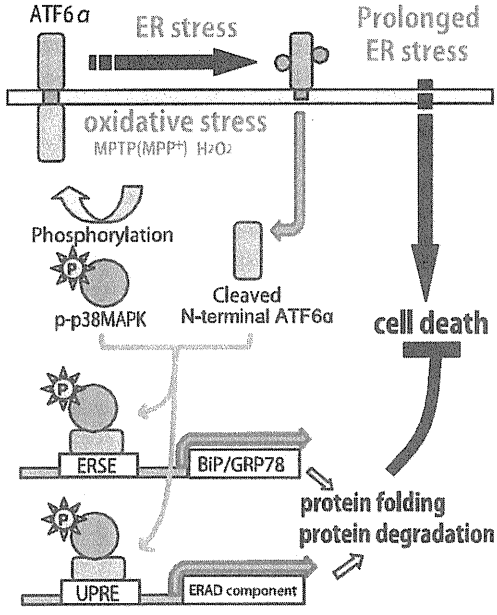

FIGURE 6. **A proposed model for oxidative stress-ER stress pathway mediated by p38MAPK-ATF6α interaction.** Oxidative stress induced by MPTP (MPP^+) or hydrogen peroxide (H_2O_2) cleaves proteolytic N-terminal fragment of ATF6α and up-regulates the phosphorylation of p38MAPK. Phosphorylated p38MAPK binds to N-terminal fragment of ATF6α and enhances ATF6α-mediated induction of ER chaperones and ERAD components. This results in the degradation of accumulated unfolded proteins and prevents ER stress-induced dopaminergic neuronal death.

various kinds of signaling cascades, including; the cell cycle, apoptosis, and cell survival. Previous studies reported that p38MAPK plays a critical role in suppressing ER stress-induced macrophage apoptosis *in vitro* and advanced lesional macrophage apoptosis *in vivo* (35). On the contrary, p38MAPK also has a pro-apoptotic role in maintaining homeostasis under various stresses. Phosphorylation of p53 following phosphorylation of p38MAPK up-regulates transcription of Bax and Puma, leading to apoptotic cell death (18). Whether p38MAPK serves as pro- or anti-apoptotic agent seems to be context-dependent.

It should be noted that p38MAPK does not activate ATF6α (Fig. 5*I*) and a p38MAPK phosphorylation inhibitor does not suppress proteolytic cleavage of N-terminal ATF6α in our *vitro* study (Fig. 4*B* and supplemental Fig. S2*A*). This suggests that neither p38MAPK nor phospho-p38MAPK initiates ATF6α-mediated UPR. Mechanism underlying oxidative stress-mediated ATF6α cleavage should be elucidated in the future.

The interaction between phosphorylated p38MAPK and cleaved N-terminal ATF6α could results in a protective effect against the vicious cycle of oxidative stress-ER stress by induction of ER chaperones and ERAD components. This p38MAPK-ATF6α interaction provides a new link between oxidative stress and ER stress. ATF6α-mediated induction of ER chaperones and ERAD components via p38MAPK pathway may provide a therapeutic target for Parkinson disease and other neurodegenerative diseases associated with protein misfolding.

REFERENCES

1. Valente, E. M., Abou-Sleiman, P. M., Caputo, V., Muqit, M. M., Harvey, K., Gispert, S., Ali, Z., Del Turco, D., Bentivoglio, A. R., Healy, D. G., Albanese, A., Nussbaum, R., González-Maldonado, R., Deller, T., Salvi, S., Cortelli, P., Gilks, W. P., Latchman, D. S., Harvey, R. J., Dallapiccola, B., Auburger, G., and Wood, N. W. (2004) *Science* **304,** 1158–1160
2. Imai, Y., Soda, M., Inoue, H., Hattori, N., Mizuno, Y., and Takahashi, R. (2001) *Cell* **105,** 891–902
3. Uehara, T., Nakamura, T., Yao, D., Shi, Z. Q., Gu, Z., Ma, Y., Masliah, E., Nomura, Y., and Lipton, S. A. (2006) *Nature* **441,** 513–517
4. Wang, H. Q., Imai, Y., Inoue, H., Kataoka, A., Iita, S., Nukina, N., and Takahashi, R. (2008) *J. Neurochem.* **107,** 171–185
5. Trojanowski, J. Q., and Lee, V. M. (1998) *Arch. Neurol.* **55,** 151–152
6. Mori, K. (2000) *Cell* **101,** 451–454
7. Yamamoto, K., Sato, T., Matsui, T., Sato, M., Okada, T., Yoshida, H., Harada, A., and Mori, K. (2007) *Dev. Cell* **13,** 365–376
8. Wu, J., Rutkowski, D. T., Dubois, M., Swathirajan, J., Saunders, T., Wang, J., Song, B., Yau, G. D., and Kaufman, R. J. (2007) *Dev. Cell* **13,** 351–364
9. Rutkowski, D. T., Wu, J., Back, S. H., Callaghan, M. U., Ferris, S. P., Iqbal, J., Clark, R., Miao, H., Hassler, J. R., Fornek, J., Katze, M. G., Hussain, M. M., Song, B., Swathirajan, J., Wang, J., Yau, G. D., and Kaufman, R. J. (2008) *Dev. Cell* **15,** 829–840
10. Haze, K., Okada, T., Yoshida, H., Yanagi, H., Yura, T., Negishi, M., and Mori, K. (2001) *Biochem. J.* **355,** 19–28
11. Nadanaka, S., Yoshida, H., Kano, F., Murata, M., and Mori, K. (2004) *Mol. Biol. Cell* **15,** 2537–2548
12. Adachi, Y., Yamamoto, K., Okada, T., Yoshida, H., Harada, A., and Mori, K. (2008) *Cell Struct. Funct.* **33,** 75–89
13. Yoshida, H., Haze, K., Yanagi, H., Yura, T., and Mori, K. (1998) *J. Biol. Chem.* **273,** 33741–33749
14. Haze, K., Yoshida, H., Yanagi, H., Yura, T., and Mori, K. (1999) *Mol. Biol. Cell* **10,** 3787–3799
15. Yokoyama, H., Kuroiwa, H., Yano, R., and Araki, T. (2008) *Neurol. Sci.* **29,** 293–301
16. Eisenhofer, G., Kopin, I. J., and Goldstein, D. S. (2004) *Pharmacol. Rev.* **56,** 331–349
17. Junn, E., and Mouradian, M. M. (2001) *J. Neurochem.* **78,** 374–383
18. Karunakaran, S., Saeed, U., Mishra, M., Valli, R. K., Joshi, S. D., Meka, D. P., Seth, P., and Ravindranath, V. (2008) *J. Neurosci.* **28,** 12500–12509
19. Gomez-Lazaro, M., Galindo, M. F., Concannon, C. G., Segura, M. F., Fernandez-Gomez, F. J., Llecha, N., Comella, J. X., Prehn, J. H., and Jordan, J. (2008) *J. Neurochem.* **104,** 1599–1612
20. Newhouse, K., Hsuan, S. L., Chang, S. H., Cai, B., Wang, Y., and Xia, Z. (2004) *Toxicol. Sci.* **79,** 137–146
21. Thuerauf, D. J., Arnold, N. D., Zechner, D., Hanford, D. S., DeMartin, K. M., McDonough, P. M., Prywes, R., and Glembotski, C. C. (1998) *J. Biol. Chem.* **273,** 20636–20643
22. Yamamoto, K., Yoshida, H., Kokame, K., Kaufman, R. J., and Mori, K. (2004) *J. Biochem.* **136,** 343–350
23. Yamamoto, K., Suzuki, N., Wada, T., Okada, T., Yoshida, H., Kaufman, R. J., and Mori, K. (2008) *J. Biochem.* **144,** 477–486
24. Holtz, W. A., and O'Malley, K. L. (2003) *J. Biol. Chem.* **278,** 19367–19377
25. Ryu, E. J., Harding, H. P., Angelastro, J. M., Vitolo, O. V., Ron, D., and Greene, L. A. (2002) *J. Neurosci.* **22,** 10690–10698
26. Silva, R. M., Ries, V., Oo, T. F., Yarygina, O., Jackson-Lewis, V., Ryu, E. J., Lu, P. D., Marciniak, S. J., Ron, D., Przedborski, S., Kholodilov, N., Greene, L. A., and Burke, R. E. (2005) *J. Neurochem.* **95,** 974–986
27. Fornai, F., Schlüter, O. M., Lenzi, P., Gesi, M., Ruffoli, R., Ferrucci, M., Lazzeri, G., Busceti, C. L., Pontarelli, F., Battaglia, G., Pellegrini, A., Nicoletti, F., Ruggieri, S., Paparelli, A., and Südhof, T. C. (2005) *Proc. Natl. Acad. Sci. U.S.A.* **102,** 3413–3418
28. Shimoji, M., Zhang, L., Mandir, A. S., Dawson, V. L., and Dawson, T. M. (2005) *Brain Res. Mol. Brain Res.* **134,** 103–108
29. Holtz, W. A., Turetzky, J. M., Jong, Y. J., and O'Malley, K. L. (2006)

J. Neurochem. **99,** 54–69
30. Haynes, C. M., Titus, E. A., and Cooper, A. A. (2004) *Mol. Cell* **15,** 767–776
31. Malhotra, J. D., Miao, H., Zhang, K., Wolfson, A., Pennathur, S., Pipe, S. W., and Kaufman, R. J. (2008) *Proc. Natl. Acad. Sci. U.S.A.* **105,** 18525–18530
32. Du, Y., Ma, Z., Lin, S., Dodel, R. C., Gao, F., Bales, K. R., Triarhou, L. C., Chernet, E., Perry, K. W., Nelson, D. L., Luecke, S., Phebus, L. A., Bymaster, F. P., and Paul, S. M. (2001) *Proc. Natl. Acad. Sci. U.S.A.* **98,** 14669–14674
33. Luo, S., and Lee, A. S. (2002) *Biochem. J.* **366,** 787–795
34. Hung, C. C., Ichimura, T., Stevens, J. L., and Bonventre, J. V. (2003) *J. Biol. Chem.* **278,** 29317–29326
35. Seimon, T. A., Wang, Y., Han, S., Senokuchi, T., Schrijvers, D. M., Kuriakose, G., Tall, A. R., and Tabas, I. A. (2009) *J. Clin. Invest.* **119,** 886–898